CHALMERS
UNIVERSITY OF TECHNOLOGY

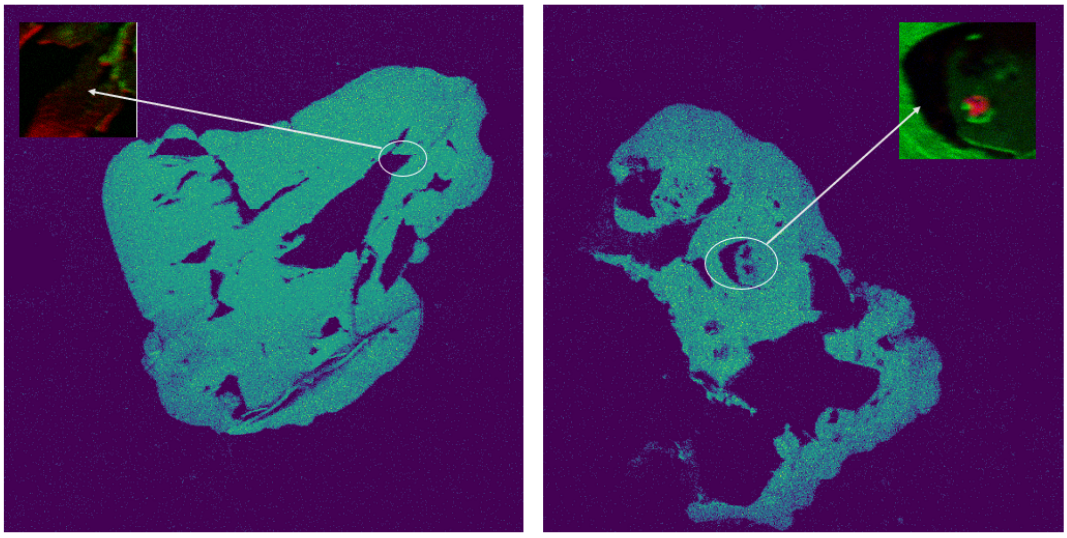

Isotopic analysis in cancer cells and tissues by Mass Spectrometry

Master's Thesis in Materials Chemistry

AQILA NASERI

DEPARTMENT OF CHEMISTRY AND CHEMICAL ENGINEERING
CHALMERS UNIVERSITY OF TECHNOLOGY
Gothenburg, Sweden 2025
www.chalmers.se

Master's thesis 2025

Isotopic analysis in cancer cells and tissues by Mass Spectrometry

AQILA NASERI

CHALMERS
UNIVERSITY OF TECHNOLOGY

Department of chemistry and chemical engineering
Division of chemistry and biochemistry
Chalmers University of Technology
Gothenburg, Sweden 2025

Isotopic analysis in cancer cells and tissues by Mass Spectrometry
AQILA NASERI

Supervisor: Per Malmberg
Examiner: Per Malmberg

Master's Thesis 2025
Department of chemistry and chemical engineering
Division of chemistry and biochemistry
Chalmers University of Technology
SE-412 96 Gothenburg
Telephone +46 31 772 1000

Cover: 2D ToF-SIMS image of chicken embryo samples obtained through large-area analysis showing spatial ion distribution.

Typeset in LaTeX
Printed by Chalmers Reproservice
Gothenburg, Sweden 2025

Isotopic analysis in cancer cells and tissues by Mass Spectrometry

AQILA NASERI
Department of chemistry and chemical engineering
Chalmers University of Technology

Abstract

Early detection and treatment of cancer can significantly reduce mortality rates. One promising approach is the use of biomarkers based on metal element isotopic fractionation. Previous studies have shown that elements such as zinc and calcium exhibit characteristic isotopic shifts in cancer tissues and body fluids.

In this project, time-of-flight secondary ion mass spectrometry (ToF-SIMS) was used to analyze the isotopic fractionation of zinc, iron, calcium, copper, and magnesium associated with cancer. Human breast cancer cell lines and chicken embryo models were used as samples. The results demonstrated clear isotopic fractionation in treated and untreated cancer cell samples for calcium, magnesium, iron, and zinc. In chicken embryo tissues, zinc and iron were not detectable at a concentration of 10 µg/mL using ToF-SIMS, while copper isotopes were consistently detected in both treated and untreated samples. These observations suggest that isotopic fractionation of certain metal elements has strong potential as a biomarker for cancer detection. However, it is worth mentioning that potential sources of error may have contributed to the limited detection of Fe and Zn signals, and further methodological improvements and research are needed to draw definitive conclusions.

Furthermore, ToF-SIMS proved to be a semi-quantitative tool capable of probing isotopic patterns in tissues and cells and providing relative quantification of metal elements under certain conditions. Further optimization is needed to determine the most suitable conditions for tissue analysis using ToF-SIMS. Overall, this study highlights the promising role of metal isotopic fractionation in cancer diagnostics and the utility of ToF-SIMS in biological analysis.

Keywords: Trace metals, Isotopic fractionation, Cancer biomarkers, Cancer cells, Chicken embryo, Mass spectrometry, ToF-SIMS.

Acknowledgements

I would like to express my deepest gratitude to my supervisor and examiner, Per Malmberg, for his guidance, support, and encouragement throughout the course of this thesis. His expertise and thoughtful insights have been invaluable to my work and learning. I am also sincerely thankful to Elias Ranjbari for his generous help with the TOF-SIMS and for always being willing to share his knowledge and time.

A big thank you to everyone in Per Malmberg's research group, Caroline Lööf, Nivedetha Venkatraman, and Robin Rydbergh, for creating such a supportive and inspiring environment. Your collaboration and kindness made this journey not only productive but also truly enjoyable. I would also like to acknowledge the entire Chemistry and Biochemistry division. It has been a privilege to work and learn alongside all of you

Finally, I would like to thank Qicheng Wu and Emma Hammarlund from Lund University for their support and guidance throughout the project.

Aqila Naseri, Gothenburg, July 2025

List of Acronyms

Below is the list of acronyms used throughout this thesis, listed in alphabetical order:

ATP	Adenosine Triphosphate
CI	Chemical Ionization
DMEM	Dulbecco's Modified Eagle's Medium
DMSO	Dimethyl Sulfoxide
ESI	Electrospray Ionization
FBS	Fetal Bovine Serum
GCIB	Gas Cluster Ion Beam
HCC 1806	Human Triple-Negative Breast Cancer Cell Line
LMIG	Liquid Metal Ion Gun
MALDI	Matrix-Assisted Laser Desorption/Ionization
MCR	Multivariate Curve Resolution
m/z	Mass-to-Charge Ratio
PBS	Phosphate-Buffered Saline
PET	Positron Emission Tomography
PFA	Paraformaldehyde
RIPA	Radioimmunoprecipitation Assay
SNR	Signal-to-Noise Ratio
ToF-SIMS	Time-of-Flight Secondary Ion Mass Spectrometry
δE	Isotopic fractionation of element E

Contents

List of Figures

List of Tables

1
Introduction

Around 10 million cancer-related deaths were reported globally in 2022, making cancer one of the deadliest diseases worldwide [1]. A major contributor to its high mortality rate is the fact that many cases are diagnosed at an advanced stage. However, early detection can significantly improve survival rates [2].

A highly promising approach for early cancer detection and treatment is the use of biomarkers, biomolecules that signal healthy or diseased conditions and biological processes in the body. Biomarkers include proteins, nucleic acids such as DNA and RNA, and specific antibodies [3]. In addition to molecular markers, the study of isotopic fractionation in tissues or body fluids is emerging as a powerful tool for cancer detection.

Essential trace metals play a critical role in metabolic processes within the human body. The metabolic reprogramming associated with many diseases leads to variations in the isotopic abundance of these metal elements, which can be effectively probed with current technologies. Examples of such diseases include diabetes and cancer [4]. The rates of biochemical processes are influenced by the mass of the elements involved. In growing tumor tissues, certain isotopes are preferentially utilized to meet specific energy demands, resulting in variations in isotopic signatures between healthy and diseased tissues [5]. This phenomenon, known as isotopic fractionation, has gained significant attention in cancer research as a tool for understanding and monitoring the disease [4]. The connection between calcium isotopic composition and bone marrow cancer is an important example of the application of natural isotope fractionation in cancer studies. Further research has shown isotopic enrichment of lighter zinc isotopes in breast tumors compared to healthy breast tissue [6].

This project will investigate elemental changes, including isotopic variations, in cancer cells and chicken embryo models that serve as tumor-like tissue environments, using Time-of-Flight Secondary Ion Mass Spectrometry (ToF-SIMS). The elements analyzed in cancer cell samples will include zinc (Zn), magnesium (Mg), calcium (Ca), and iron (Fe). In chicken embryo tissue samples, zinc (Zn), iron (Fe), and copper (Cu) will be studied.

1.1 Goal

The primary goal of this project is to investigate elemental changes, including isotopic variations, in cancer cells and chicken embryo models that simulate tumor-like tissue environments. Specifically, the project aims to:

- Develop metal standards for precise quantification and spatial mapping of metal elements within tissue and cell samples.
- Study and analyze the isotopic composition of cancer cells and chicken embryo tissues.

The elements studied in cancer cell samples include zinc (Zn), magnesium (Mg), calcium (Ca), and iron (Fe), while in chicken embryo samples, zinc (Zn), iron (Fe), and copper (Cu) are analyzed.

1.2 Delimitation

This project has several delimitations. Sample preparation for cell culturing is conducted by biology researchers at Lund University of Technology and, therefore, falls outside the direct scope of this study. However, the cell sample preparation steps are still described and included in the report. In contrast, tissue sample preparation is fully covered within the scope of this work. Electroporation has been selected as the technique for facilitating the penetration of metal elements into the samples.

The analytical focus of this project is limited to five specific elements: zinc (Zn), magnesium (Mg), calcium (Ca), iron (Fe), and copper (Cu). The primary analytical technique employed throughout this study is Time-of-Flight Secondary Ion Mass Spectrometry (ToF-SIMS).

1.2.1 Specification of the issue being investigated

The central research question of this project is: How do specific isotopic variations correlate with tumor progression, and can these changes serve as reliable biomarkers for the early detection and characterization of cancer?
To address this question, the project will be conducted in the following stages:

- Development and analysis of Metal Standards: Metal standards will be prepared by adding metal solutions to cell debris. The cell type used for this purpose is HCC1806 (a human breast cancer cell line). These standards are crucial for the accurate quantification of metals within cancer cells.

- Chicken Embryo Model: Chicken embryos will serve as an intermediate model for developing metal standards within a tissue environment. This model provides a controlled biological system to study the isotopic distribution of elements in tumor-like tissues.

2

Theory

This section explores the biological and chemical foundations of cancer, as well as the role of metal ions in cellular function. It introduces the fundamentals of isotopic effects and fractionation, including how these properties change during tumor development. The mass spectrometry methods used to study these transformations, particularly ToF-SIMS, are explained. In addition, sample preparation techniques, including electroporation, are discussed.

2.1 Role of metal elements in human body

The human body relies on essential elements to function and carry out metabolic processes. Among these are metal elements that play important roles in maintaining proper cellular activity. These are referred to as *essential metal elements*, defined as metals that are naturally present in human tissues and whose absence or deficiency can cause damage to organs and impair physiological functions. Essential metal elements include sodium (Na), potassium (K), magnesium (Mg), calcium (Ca), manganese (Mn), iron (Fe), cobalt (Co), copper (Cu), zinc (Zn), and molybdenum (Mo) [7]. In this project, the focus is on five of these: calcium (Ca), zinc (Zn), copper (Cu), iron (Fe), and magnesium (Mg).

2.1.1 Calcium

Calcium (Ca) is one of the most important inorganic elements in the human body. While it is a major component of bones and teeth, it also plays vital roles in various enzymatic processes and cell signaling pathways, including those involved in muscle contraction and nerve function. Moreover, this metal element is essential for maintaining blood pH stability and regulating cell division [7].

2.1.2 Zinc

Zinc (Zn) is one of the most important d-block metal ions in the human body, found in high concentrations in the brain, bones, and muscles. It is involved in numerous enzymatic reactions and plays crucial roles in cellular processes as a catalyst, regulator, and structural component. Zinc deficiency can lead to a weakened immune system and delayed development [7].

2.1.3 Copper

Copper (Cu) is an essential metal element involved in various enzymatic reactions in the body. It plays an important role in the formation of structural tissues such as collagen and keratin. Both copper overload and deficiency can lead to a range of health problems, including mental and developmental disorders, as well as life-threatening conditions such as Wilson's disease [7].

2.1.4 Iron

Iron (Fe) is one of the most essential elements for all living organisms. In the human body, more than 500 gene-encoded proteins contain iron. This metal is involved in numerous enzymatic reactions and plays critical roles in oxygen transport, electron transfer, and nucleic acid synthesis. Both iron deficiency and overload can disrupt cellular processes and lead to various health issues [7].

2.1.5 Magnesium

Magnesium (Mg) is another important cation in human tissue, involved in various intracellular and enzymatic reactions. This essential metal plays a key role in the synthesis of fatty acids and proteins, as well as in metabolic processes related to ATP formation. Furthermore, magnesium is a vital component of the skeletal and muscular systems and contributes to the regulation of the immune system [7].

2.1.6 Isotopes and Isotopic Fractionation

Atoms with the same atomic number but different atomic masses are called isotopes. The difference in atomic mass arises from variations in the number of neutrons in the atomic nucleus. Isotopes can occur in different proportions, known as isotopic abundances. In particular, natural abundance refers to the relative amount of each isotope of an element as it occurs naturally on earth [8].

When an element participates in a chemical or physical reaction, isotopic fractionation can occur. This refers to the process in which one isotope of an element is preferentially utilized or enriched over others. Typically, lighter isotopes are more readily incorporated into reaction products due to differences in reaction rates between light and heavy isotopes. Such fractionation commonly arises in processes like evaporation, diffusion, and various biological reactions.

Isotopic fractionation, which quantifies the difference between the isotope ratio in a sample and that in a reference standard, is expressed by delta δ. notation. The value is reported in ‰ and calculated using the following formula:

$$\delta^x E = \left(\frac{R_{\text{sample}}}{R_{\text{standard}}} - 1 \right) \times 1000 \tag{2.1}$$

where $R = \frac{xE}{yE}$ is the ratio of the heavier isotope (xE) to the lighter isotope (yE) of an element E. The factor of 1000 converts the result to parts per thousand (‰)

clled per mil. A positive δ value refers to enrichment in the heavier isotope relative to the standard, while a negative value shows depleteion in the heavier isotope [9].

2.2 Principles of cancer biology

Cancer is a disease marked by uncontrolled growth and spread of abnormal cells. Under normal conditions, cells grow and multiply to replace old or damaged cells that die. However, in cancer, this process changes, and abnormal or damaged cells continue to grow and form tumors [10]. Cancer cells change their metabolism to promote their growth and survival, primarily through increased glucose uptake. This phenomenon is known as the Warburg effect, which will be discussed in greater detail later. [5].

2.2.1 Isotopic Fractionation in Cancer

The concept of isotopic fractionation is a central phenomenon in geochemistry and has also become a powerful tool in biomedical research. In biological systems, cellular metabolism undergoes significant reprogramming under conditions such as neurological diseases, diabetes, and cancer. These changes lead to noticeable variations in isotope utilization during biochemical reactions. Because the energy demand of the reaction depends on the mass of the involved reactants, certain isotopes are preferentially used in metabolic pathways. This selective process results in measurable isotopic fractionation [6]. The approach is now widely used to study human health and disease and is gaining significant attention in cancer research, where isotopic fractionation has the potential to be used as a biomarker for early cancer detection or for monitoring treatment response [4].

Studies have shown a strong correlation between isotopic fractionation of specific metal elements and various cancer types. One notable example is the relationship between calcium isotopic composition and bone marrow cancer (myeloma) [4]. In breast cancer, early-stage tumor tissues exhibit an enrichment of lighter zinc isotopes, with higher levels of ^{64}Zn relative to ^{66}Zn [6]. This suggests that tumor cells may prefer lighter isotopes due to reprogramming of metal metabolism. Copper isotopic composition also has the potential to be used as a biomarker. It has been found that the serum of patients with liver cirrhosis is enriched in the lighter copper isotope compared to that of healthy individuals [4]. Moreover, studies have also shown that the molecular composition of cells, including cholesterol and lipids, undergoes significant changes during tumor progression [11]. However, in this study, the focus is mainly on isotopic variation, and molecular changes remain outside the scope of the study.

In cancer cells, isotopic fractionation may stem from underlying metabolic reprogramming, including phenomena such as the Warburg effect, which will be discussed in the next section.

2.2.1.1 Warburg Effect

The Warburg effect, one of the main characteristics of cancer, was first identified by Otto Warburg in the 1920s. This phenomenon describes how cancer cells undergo a distinct metabolic variation, where they mainly rely on glycolysis even when oxygen is present [12]. In healthy cells, glucose is first broken down into pyruvate, a three-carbon molecule essential for metabolism, through glycolysis [13]. In the presence of oxygen, most pyruvate is further oxidized in the mitochondria via oxidative phosphorylation, producing carbon dioxide. However, when oxygen is absent, cells convert pyruvate into lactate through anaerobic glycolysis [14].

Warburg discovered that, unlike normal cells, cancer cells convert most of their glucose into lactate, even in the presence of oxygen. This shift, known as aerobic glycolysis, is less efficient in terms of adenosine triphosphate (ATP) production. ATP is an energy-carrying molecule that stores and releases energy to power cellular processes [15]. The aerobic process produces approximately 18 times less energy per glucose molecule compared to oxidative phosphorylation [14]. Despite their lower efficiency in energy production, cancer cells compensate by consuming more glucose. This increased glucose uptake is studied in Positron Emission Tomography (PET), a powerful imaging technique used to visualize biochemical and physiological processes in living organisms [16]. Today, the technique is mainly used to study cellular metabolism and molecular activity in the brain, heart, and to monitor cancerous tumors [17].

Both cancer cells and normal proliferating cells continue some oxidative phosphorylation, but glycolysis dominates because it provides essential metabolic intermediates for cell division. A portion of glucose is also converted into biosynthetic pathways that support cell growth, further promoting the rapid proliferation characteristic of cancer cells. This adaptation in energy production allows tumors to thrive and grow despite the metabolic inefficiency of aerobic glycolysis [14].

2.3 Analysis Methods

This section explains the analytical method of ToF-SIMS used for the analysis of the samples, as well as the multivariate data analysis technique, Multivariate Curve Resolution (MCR), which will be applied to some of the image data obtained from ToF-SIMS.

2.3.1 Mass Spectrometry

Mass spectrometry is a vital analytical technique for characterizing chemical compounds and biological molecules by measuring the mass-to-charge ratios of ions in the gas phase. The technique was developed by British scientists Joseph John Thomson and Francis William Aston. Thomson, who discovered the subatomic particle electrons while investigating the properties of gases in an electric field, laid

the groundwork for this technology. Aston further contributed to the field by developing the first mass spectrometer, which enabled the discovery and separation of isotopes of chemical elements. Both Thomson and Aston were awarded Nobel Prizes for their groundbreaking contributions to science [18].

The main principle of mass spectrometry (MS) involves ionizing inorganic or organic compounds, then separating these ions by their mass-to-charge ratio (m/z), and finally detecting them both qualitatively and quantitatively based on these values and their relative abundances. A typical mass spectrometer operates under high vacuum conditions and includes three main components: an ion source, a mass analyzer, and a detector [18].

The ion source, as the name implies, is a component of the mass spectrometer that converts neutral gaseous molecules into ions. One of the most traditional ion sources used in mass spectrometry is electron ionization (EI). In this process, an energetic electron collides with a neutral sample, resulting in the ionization of the analyte. This typically forms what is known as the molecular ion. For ionization to occur, the kinetic energy of the incoming electron must exceed the ionization energy of the neutral species. The ionization energy is defined as the minimum energy required to remove an electron from a neutral species in its ground state [19]. In addition to electron ionization, mass spectrometry employs several other ionization sources, including chemical ionization (CI), electrospray ionization (ESI), matrix-assisted laser desorption/ionization (MALDI), and many others [20].

The mass analyzer separates the ions produced in the ion source according to their mass-to-charge ratios. The most important types of mass analyzers include quadrupole, magnetic sector, and time-of-flight (ToF) analyzers, with ToF being discussed in more detail in Section 2.3.1 [21]. Moreover, various types of detectors are employed to convert the ions received from the mass analyzer into measurable signals. Three common types of detectors are the Faraday cup, the electron multiplier, and the scintillation counter [22].

2.3.1.1 ToF-SIMS

Time-of-Flight Secondary Ion Mass Spectrometry (ToF-SIMS) is a specialized type of mass spectrometry used to characterize material composition and analyze surface chemistry. The technique operates by directing a highly focused beam of primary ions onto the surface of a sample. This ion beam interacts with the sample, ionizing surface molecules and generating secondary ions—hence the name of the technique. These secondary ions are extracted and directed into a mass analyzer, which separates them based on their mass-to-charge ratio (m/z) [23].

A Time-of-Flight (ToF) analyzer is a specific type of mass analyzer that measures the time it takes for each ion to travel a fixed distance, known as the "time of flight." Since ions with the same kinetic energy but different masses travel at different velocities, lighter ions reach the detector faster than heavier ones. This allows for the precise identification of atoms and molecules present on the surface of the sample [21].

ToF-SIMS is capable of detecting all elements in the periodic table. It provides a range of valuable information, including mass spectral data, two-dimensional (2D) chemical images of the sample surface, and depth profiling, which enables three-dimensional (3D) chemical distribution analysis. An example of a commonly used primary ion in ToF-SIMS is the bismuth ion [23].

In time-of-flight secondary ion mass spectrometry, one of the main challenges is the matrix effect. This refers to the fact that the ion signal intensity of a component in a sample depends on the material surrounding that species, which makes it difficult to convert the signal or ion intensity into a quantitative measurement of the sample's composition. For inorganic materials, a reference sample with a known concentration is typically used to quantify other samples. However, for organic materials, this approach is often impractical because they consist of many different combinations of components, making it difficult to define a single suitable reference matrix.

In this project, the analysis focuses on metal elements. For cancer cell samples, a reference sample with a known concentration of metal elements is used to obtain semi-quantitative data. For chicken embryo samples, similar metal elements are analyzed to compare the matrix effect in two different environments [24].

2.3.2 Multivariate Curve Resolution (MCR)

Multivariate Curve Resolution (MCR) is a mathematical data analysis model used to extract the pure contributions of individual components from complex mixtures. It allows for the deconvolution of overlapping signals without requiring prior knowledge about the composition or nature of the mixture [25]. In this project, the built-in MCR function of SURFACE LAB software (version 7.1, ION-TOF GmbH) is utilized to separate the contributions of each ion signal (peak) from complex spectra obtained from tissue or cell samples. The data are binned into factors that represent different groups of molecules.

2.4 Electroporation

Electroporation is a technique that increases the permeability of cell membranes, allowing for the introduction of substances such as nucleic acids and proteins into cells. This process involves applying an external electric field strong enough to generate a transmembrane voltage, which enhances the conductivity and permeability of the cell membrane. Consequently, local pores or defects form in the cytoplasmic membrane, enabling the entry of ions and molecules that typically cannot pass through the membrane [26].

In this project, electroporation will be used to introduce metal elements into cells and tissues to establish references for studying isotopic variations of metal elements in the mentioned biological systems.

2.4.1 Solvents

In this project, different types of solvents were used for sample preparation, including Phosphate-Buffered Saline (PBS), Paraformaldehyde (PFA), and Dimethyl Sulfoxide (DMSO), which are described in this section.

2.4.1.1 Phosphate-Buffered Saline (PBS)

Phosphate-buffered saline consists of various salts dissolved in water, with a pH between 7.0 and 7.4. It is a non-toxic solution commonly used in cell culture to prevent cell rupture and damage. PBS is also used for the fixation of cell samples [27].

2.4.1.2 Paraformaldehyde (PFA)

Paraformaldehyde has the chemical formula $HO(CH_2O)_nH$ and a molecular weight of 30.03 g/mol (as a monomer) [28]. It is widely used as a fixation agent for cells and tissues. PFA cross-links biomolecules through covalent bonding, resulting in a stabilized structure with enhanced mechanical properties. Studies have shown that the cell surface of fixed cells is stiffer and exhibits more uniform mechanical properties compared to unfixed cells [29].

2.4.1.3 Dimethyl Sulfoxide (DMSO)

Dimethyl sulfoxide consists of a polar sulfoxide group and two hydrophobic methyl groups. It has the chemical formula C_2H_6OS (see Figure 2.1) and a molecular weight of 78.13 g/mol [30]. The combination of hydrophilic and hydrophobic characteristics allows DMSO to dissolve both polar and non-polar substances, making it highly effective at overcoming hydrophobic barriers. Research has shown that DMSO can increase cell membrane permeability and enhance the penetration of elements and drugs across biological membranes [31].

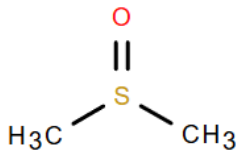

Figure 2.1: Chemical structure of dimethyl sulfoxide (DMSO)

2.4.2 Phosphorylcholine

N,N,N-trimethyl-2-(phosphonooxy)ethanaminium, known as phosphorylcholine or phosphocholine, is a key component of the cell membrane. It has the chemical formula $C_5H_{15}NO_4P$ and consists of a negatively charged phosphate group and a positively charged choline group [32]. Phosphorylcholine is found in the cells of

both eukaryotes and prokaryotes. Its molecular weight is 184.15 g/mol, and in its cationic form [$C_5H_{15}NO_4P^+$], which appears at m/z 184 in mass spectrometry [33]. In this project, the phosphocholine cation is used as a marker to confirm that the analyzed region corresponds to cancer cells or chicken embryo tissue.

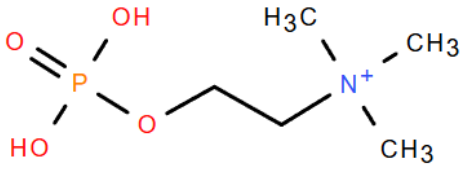

Figure 2.2: Chemical structure of phosphorylcholine

3
Methods

The methodology in this report consists of two parts: a literature review and laboratory work. The literature review involves gathering information from various articles and reports on the principles of cancer, including its elemental and molecular composition, as well as sample preparation techniques. Additionally, an in-depth study of the principles of mass spectrometry, particularly focusing on ToF-SIMS, is conducted. The laboratory part begins with sample preparation at Lund University of Technology. Subsequently, the samples are studied using ToF-SIMS, and the data are analyzed.

3.1 Sample Preparation

In this study, two types of samples were used: a breast cancer cell line and chicken embryo samples, both with and without added metal standards. Since it was initially unclear which type of chicken embryo sample would be suitable for analysis with ToF-SIMS, the embryos were prepared using different methods and developmental stages, resulting in distinct sample groups.

3.1.1 Cell samples

HCC 1806 (ATCC® CRL-2335™), a human triple-negative breast cancer cell line, was cultured in Dulbecco's Modified Eagle's Medium (DMEM) containing 4.5 g/L glucose, L-glutamine, and phenol red, supplemented with 10% heat-inactivated fetal bovine serum (FBS). Cells were maintained in T-75 flasks at 37°C in a humidified incubator with 5% CO_2. Subculturing was performed at approximately 80% confluency using Gibco™ TrypLE™ Express Enzyme, following a wash with phosphate-buffered saline (PBS). Cells were routinely passaged every 3–4 days.

For ToF-SIMS sample preparation, cells were harvested and lysed using radioimmunoprecipitation assay (RIPA) buffer, prepared by diluting a 10× RIPA stock solution with Milli-Q water to obtain a 1× working concentration. The resulting lysate, containing cell debris, was divided into 1.5 mL microcentrifuge tubes. Cell debris obtained from the lysate was directly dropped onto a clean glass slide, serving as the reference cell sample. For metal standard preparation, a metal element solution was mixed into the cell debris and then similarly dropped onto the glass surface. Each droplet was 1 µL in volume and was allowed to dry

completely before the next was added. This deposition process was repeated at least six times on the same spot to ensure sufficient material accumulation.
Three sample types were prepared for each metal element. These included: a reference sample containing only cell debris without metal treatment; a sample combining cell debris with the metal standard solution; and a sample containing the metal standard solution alone, deposited directly on a glass slide. This design allowed for direct comparison between untreated cells, metal-treated cells, and metal standards. All samples were then prepared for ToF-SIMS analysis. Table 3.1 provides an overview of the cell samples.

Table 3.1: Overview of Cell Sample Types

Sample Type	**Contents**
Reference Cell Sample	Cell debris only
Standard Solution Sample	Metal standards only (Ca, Mg, Fe, Zn)
Cell + Standard Sample	Cell debris + Metal elements (Ca, Mg, Fe, Zn)

3.1.2 Chicken embryo samples

To identify the most optimal condition for chicken embryo tissue analysis in ToF-SIMS, a series of iterative preparation and analysis strategies were developed. Embryos were collected at different developmental stages and subjected to various treatment conditions. This process led to the creation of three distinct groups of samples.
These groups are not isolated experiments but rather interconnected stages in a continuous optimization process, where a particular approach that proved ineffective was modified or replaced in the next sample group. These modifications included the use of electroporation, the addition of extra solvents such as DMSO, variations in the type and concentration of metal element treatments (e.g., zinc, iron, and copper), and adjustments to the ToF-SIMS analysis techniques. Despite the differences in treatment and technique, all samples were prepared following a shared general protocol, as outlined below.

Chicken embryos were incubated for a defined period and then dissected in Ringer's solution. Embryos were fixed overnight in 4% paraformaldehyde (PFA) at 4 °C. After fixation, samples were rinsed three times in PBS, each for 30 minutes. A stepwise sucrose infiltration was then applied: 5% sucrose for 1 hour, followed by 15% sucrose for 4 hours at room temperature. Samples were subsequently transferred to 7.5% gelatin at 37 °C and incubated overnight.

Tissues were embedded in 7.5% gelatin by placing them in embedding molds pre-coated with a thin gelatin layer, then covered with freshly melted gelatin. The embedded samples were rapidly frozen by immersion in liquid nitrogen and equilibrated at –20 °C for 20 minutes. Fully frozen blocks were stored at –80 °C until sectioning. Sections of 5–20 µm thickness were cut using a cryostat at –20 °C

to –30 °C and mounted onto glass slides for ToF-SIMS analysis. Freeze-drying was then performed for at least 24 hours. After freeze-drying, samples were stored under dry conditions, avoiding contact and exposure to moisture.

While all chicken embryo samples followed the general preparation procedure described above, specific treatments and conditions were applied to generate distinct sample groups for comparative analysis. These included variations in embryo developmental stage, electroporation status, and the timing or presence of metal ion treatments. The following table summarizes the characteristics and preparation methods used for each sample group.

Table 3.2: Summary of chicken embryo sample groups and their treatment conditions.

Group Name	**Incubation Time**	**Treatment Conditions**
A	Three days	Treated with Fe and Zn standard solutions and electroporated.
B	Four days	Treated with Fe standard solution with/without DMSO and electroporated (with or without incubation).
C	Four days	Treated with Cu standard solution either before freeze-drying, after freeze-drying, or left untreated.

3.1.2.1 Group A

For this sample group, chicken embryos were incubated for three days. A drop of metal element solution (either zinc or iron) at a concentration of 10 µg/mL in 0.05% nitric acid was applied directly onto each embryo prior to dissection. Electroporation was then performed using an Electroporator Power Supply developed by the Caltech Bio-Electronics Shop. The device was configured to deliver five pulses, each lasting 50 ms, at an output voltage of 50 V.

Following electroporation, embryos were dissected, and samples were prepared according to the general procedure described in Section 3.1.2. In addition to the metal-treated embryos, one reference sample with no treatment was included for comparison. Table 3.3 summarizes the sample IDs and their corresponding treatment conditions.

Table 3.3: Overview of Chicken Embryo Samples from Group A and Treatment Conditions

Sample ID	Metal Treatment	Concentration (µg/mL)	HNO_3 (%)
A1	None (reference sample)	–	–
B1	Zn	10	0.05
A3	Fe	10	0.05

3.1.2.2 Group B

For this sample group, chicken embryos were incubated for four days prior to treatment. All samples were prepared according to the general procedure described in Section 3.1.2 and electroporated as outlined in Section 3.1.2.1. In this group, only iron (Fe) was used as the metal element. A key difference was the use of 10% dimethyl sulfoxide (DMSO) in PBS, which was mixed with the Fe standard solution at a concentration of 10 µg/mL.

Different treatment conditions were applied across the samples. Some embryos were treated with the Fe + DMSO mixture only, without further intervention. Others were electroporated after application of the mixture, and a subset of these was also incubated at 37 °C for 30 minutes post-treatment to enhance metal ion uptake. Additionally, a separate group of samples was treated with Fe alone (without DMSO), followed by electroporation and incubation, to evaluate the effect of DMSO on tissue penetration. An overview of the treatment methods applied to each Group B sample is presented in Table 3.4.

Table 3.4: Overview of Group B chicken embryo samples and their treatment methods.

Sample ID	Treatment Conditions
B1	Fe + DMSO solution only
A2	Fe + DMSO followed by electroporation and incubation
A3	Fe + DMSO solution and electroporated
A4	Fe solution, followed by electroporation and incubation

3.1.2.3 Group C

In this group, chicken eggs were incubated for four days, and the samples were prepared according to the general procedure described in Section 3.1.2. Copper (Cu) was used as the metal element; however, the Cu standard was part of a multi-element solution containing Ca and Mg at 100 µg/mL, Cu, Fe, Sr, and Zn at 10 µg/mL, and Ag, Mo, and Rb at 1 µg/mL, all dissolved in 5% HNO_3.

The solution was applied either before the freeze-drying step or afterward, just prior to ToF-SIMS analysis. Electroporation was not applied to any of the samples in

this group. Additionally, control samples without any metal solution were prepared for each incubation time point to serve as untreated references. Table 3.5 presents the sample types prepared for Group C.

Table 3.5: Overview of Group C chicken embryo samples and their treatment methods.

Sample ID	**Treatment Method**
A1	Treated with Cu standard solution after freeze-drying
B1	Treated with Cu standard solution before freeze-drying
A2	Untreated control sample
A4	Untreated control sample

3.2 ToF-SIMS Analysis

To analyze the isotopic structure of metal elements in cell and tissue samples, time-of-flight secondary ion mass spectrometry (ToF-SIMS) was employed as the primary analytical technique. A TOF.SIMS 5 system (ION-TOF GmbH, Münster, Germany) equipped with a bismuth (Bi_3^+) liquid metal ion gun (LMIG) at 25 keV as the primary ion source and an argon gas cluster ion beam (GCIB) at 5 keV for sputtering was used. The primary ion current was approximately 0.3–0.4 pA. Analyses were conducted in spectroscopy mode (SM) using the Bi_3^+ beam, and spectra were recorded in positive ion mode.

Mass calibration of the acquired spectra was performed using characteristic elemental and fragment ions, including [C^+], [CH^+], [$CH_2{}^+$], [$CH_3{}^+$], and other confidently identified peaks. Data processing was carried out using SurfaceLab software (version 7.1, ION-TOF GmbH). Depending on the sample type, both 2D imaging and depth profiling (3D analysis) were performed. For cell samples, 2D analysis was conducted in automated mode, while for chicken embryo tissue samples, both 2D and depth profiling modes were applied.

To further investigate chemical variability within selected samples, Multivariate Curve Resolution (MCR) analysis was applied using the built-in MCR function in SurfaceLab software. Spectra and 2D ToF-SIMS images from specific regions of interest were selected for this analysis. The peak search function in SurfaceLab was used to extract peaks within the m/z 10–200 range, filtering for ion counts exceeding 100 and a signal-to-noise ratio (SNR) greater than 1. MCR analysis was then performed using 10 factors, which were determined to be optimal for identifying the chemical composition and spatial variation within the samples. Detailed acquisition settings for each procedure are described in the following sections.

3.2.1 Cell Samples

Cancer cell samples were analyzed in automated mode with 2D imaging. A total area of 500 µm × 500 µm was scanned for each measurement using the LMIG system with Bi_3^+ as the primary ion source. Six regions were measured per sample. All analyses were performed in positive ion mode.

3.2.2 Chicken Embryo Samples

ToF-SIMS analyses were performed on chicken embryo samples based on their group classification. All samples were analyzed using the same instrument, as described in Section 3.2.1. Group A samples were analyzed following the same procedure as the cell samples, using 2D imaging. However, some were also analyzed in 3D mode by sputtering with an argon gas cluster ion beam (GCIB, 5 keV) to access deeper layers and remove surface contaminants.

Spectra were recorded in positive ion mode using the LMIG with Bi_3^+ as the primary ion source. The primary ion current was approximately 0.3–0.5 pA. Group B samples were analyzed using 2D large-area analysis in raster stage scan mode, with six shots per pixel to cover the entire tissue area. Images of 3–5 mm^2 were acquired at a resolution of 256 × 256 pixels. For Group C, both 2D large-area analysis and standard 2D imaging were performed, including sputtering when required.

3.2.3 Isotopic Fractionation Calculation of Cell Samples

For each element studied, isotopic fractionation was calculated using ToF-SIMS data. The ion counts of the heavier and lighter isotopes were recorded for six replicates per sample type, including untreated cell samples, cells treated with a metal standard solution, and the standard solution alone.

From these counts, the isotope ratio ($R = \frac{xE}{yE}$), where xE is the heavier isotope and yE is the lighter isotope, was calculated for each replicate. The mean isotope ratio for each sample group was then determined and used in Equation 2.1 to calculate isotopic fractionation (δ). This value is expressed in parts per thousand (‰), also referred to as per mil. A positive δ value indicates enrichment in the heavier isotope relative to the standard, while a negative value indicates enrichment in the lighter isotope.

4

Results and Discussion

This section is organized into two main parts: the results obtained from the cancer cell samples and those derived from the chicken embryo samples. These findings are subsequently discussed in the context of relevant theoretical frameworks and the data analysis techniques employed.

4.1 Cancer cell samples

The cell samples are grouped into three types: reference cells, cells treated with a standard metal solution, and the metal standard solution alone. For each metal studied, the results are presented in separate tables that include the calculated ratios between lighter and heavier isotopes of each metal. These ratios are then used in equation (2.1) to determine the degree of isotopic fractionation, expressed as enrichment or depletion in per mil (‰) relative to the standard. The tables provide a direct comparison among untreated cells, treated cells, and the standards.

Isotopic analysis of zinc in the cancer cells reveals a clear depletion of the heavier zinc isotope. Specifically, cancer cells showed a δ^{66}Zn value of –223‰ relative to the Zn standard, indicating a preference for the lighter isotope. When zinc solution was added to the cells, this fractionation became even more pronounced, with a δ^{66}Zn value of –424‰. Table 4.1 shows the isotopic fractionation of zinc (Zn).

Table 4.1: Isotopic fractionation of zinc (Zn) in cell samples

Sample	**Avg ^{66}Zn/^{64}Zn**	**δ^{66}Zn (‰)**	**Interpretation**
Cell	0.7094	–223	Slight depletion in ^{66}Zn
Zn Standard	0.9130	0	Reference
Cell + Zn	0.5260	–424	Stronger depletion in ^{66}Zn

These findings align with observations reported in the literature, where early-stage breast cancer tissues exhibit an enrichment of lighter zinc isotopes, characterized by higher levels of ^{64}Zn relative to ^{66}Zn. This isotopic signature reflects a metabolic adaptation in tumor cells, which preferentially incorporate lighter zinc isotopes during rapid growth and proliferation, and it has the potential to serve as a diagnostic marker for tumor activity or progression.

When it comes to the calcium isotope analysis, the untreated cancer cells showed a δ^{44}Ca value of +1186‰ relative to the Ca standard, indicating a significant

enrichment in the heavier isotope. When calcium was added externally to the cells, this enrichment increased further to +2532‰. These results highlight the ability of cancer cells to preferentially incorporate heavier calcium isotopes under both normal and elevated calcium conditions. This strong correlation has also been reported in the literature, particularly regarding the relationship between calcium isotopic composition and bone marrow cancer (myeloma). Table 4.2 shows the isotopic fractionation of calcium.

Table 4.2: Calcium Isotopic Fractionation in Cell Samples

Sample Group	**Avg ^{44}Ca/^{40}Ca**	**δ^{44}Ca (‰)**	**Interpretation**
Cell	0.05004	+1186	Significant enrichment in ^{44}Ca
Ca Standard	0.02288	0	Reference
Cell + Ca	0.08083	+2532	Very strong enrichment in ^{44}Ca

The iron (Fe) isotopic compositions show clear variation between the experimental conditions. Untreated cancer cells exhibited a δ^{56}Fe value of –789‰ relative to the Fe standard, indicating substantial depletion in the heavier isotope. When external iron was introduced, the δ^{56}Fe value shifted to –116‰, reflecting a moderated but still notable depletion. Table 4.3 shows the isotopic fractionation of iron.

Table 4.3: Iron Isotopic Fractionation in Cell Samples

Sample Group	**Avg ^{56}Fe/^{54}Fe**	**δ^{56}Fe (‰)**	**Interpretation**
Cell	3.9202	–789	Significant depletion in ^{56}Fe
Fe Standard	18.6031	0	Reference
Cell + Fe	16.4466	–116	Moderate depletion in ^{56}Fe

The magnesium isotope ratios show distinct isotopic fractionation. The untreated cell group displayed a δ^{26}Mg value of –659‰ compared to the Mg standard, indicating significant depletion of the heavier isotope. In contrast, the cell group treated with magnesium exhibited a δ^{26}Mg value of +33‰, suggesting moderate enrichment. The different isotopic fractionation patterns, in the form of depletion or enrichment, can be influenced by potential sources of analytical error, such as calibration inaccuracies or other methodological limitations. Table 4.4 shows the isotopic fractionation of magnesium.

Table 4.4: Magnesium Isotopic Composition in Cell Samples

Sample Group	**Avg ^{26}Mg/^{24}Mg**	**δ^{26}Mg (‰)**	**Interpretation**
Cell	0.1316	–659	Significant depletion in ^{26}Mg
Mg Standard	0.3859	0	Reference
Cell + Mg	0.3986	+33	Moderate enrichment in ^{26}Mg

Within the scope of this project, no clear correlation between iron and magnesium isotopic fractionation and cancer was observed. However, connections between the isotopic composition of these metal elements and other diseases, such as diabetes,

have been reported. Additionally, iron and magnesium deficiency or overload has been linked to various metabolic and pathological conditions, which may also affect isotopic signatures.

The bar chart in Figure 4.1 visually compares the δ values for each element between treated (*Cell + Standard*) and untreated (*Cell*) cancer cells, highlighting their isotopic fractionation behavior under the two experimental conditions. A summary of the isotopic fractionation values is shown in Table A.1 in Appendix.

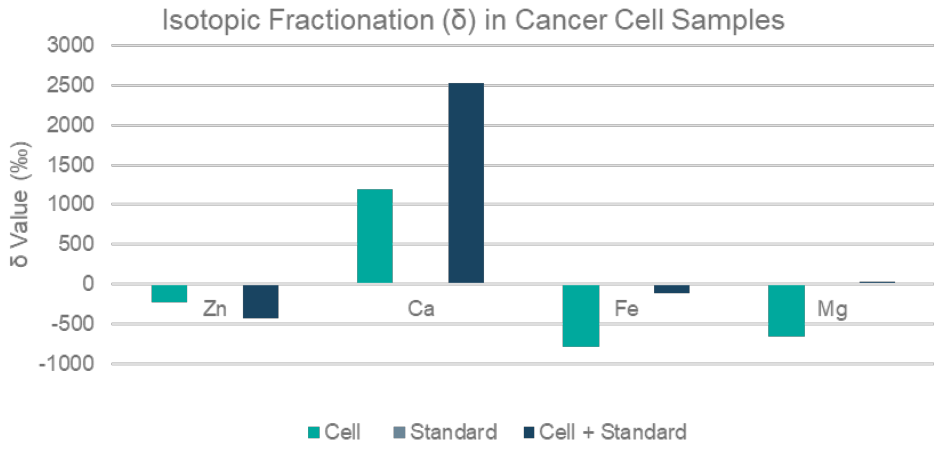

Figure 4.1: Comparison of isotopic fractionation (δ values in ‰) for Zn, Ca, Fe, and Mg across cell sample types.

From the data, it is evident that calcium exhibits a unique trend, showing strong enrichment in the heavier isotope ^{44}Ca, indicating a significant biological preference for the heavier calcium isotope. This trend is clearly visible in the chart, where calcium stands out with the highest positive δ values. In contrast, zinc and iron, show depletion in their heavier isotopes in both treated and untreated samples. Magnesium shows a marked shift from –659‰ in untreated cells to +33‰ in treated cells, suggesting a transition from depletion to slight enrichment of the heavier isotope.

Overall, the table and bar chart together reveal element-specific isotopic behaviors in cancer cells. Calcium consistently favors the heavier isotope, while zinc, iron, and magnesium initially exhibit depletion in the heavier isotopes, with distinct responses to external supplementation. These patterns may reflect biologically driven isotope fractionation mechanisms, potentially related to selective transport, uptake, or intracellular processing.

As the δ value represents a single value, the error associated with it is difficult to calculate directly. Therefore, to evaluate data accuracy, the standard error of the mean for isotopic ratio averages was calculated for each set of samples and is presented in Appendix A.1.

4.2 Chicken embryo samples

As the sample preparation and ToF-SIMS analysis of chicken embryo samples were developed through an interconnected and iterative process, the results presented for Groups A, B, and C are not isolated findings but rather part of a progressive optimization.

4.2.1 Group A

In this group, embryos were incubated for three days, treated with standard solutions of zinc and iron, and subjected to electroporation. Samples were analyzed both in 2D and 3D settings in ToF-SIMS. The samples in this group are listed in Table 4.5.

Table 4.5: Chicken Embryo Samples from Group A

Sample ID	Metal Treatment	Concentration (µg/mL)
A1	None (no treatment)	–
B1	Zn	10
A3	Fe	10

Sample A1 served as a reference chicken embryo sample without any treatment. Both zinc and iron ion signals were analyzed in this sample. Additionally, the signal corresponding to the phosphocholine cation $C_5H_{15}NO_4P^+$ was monitored at m/z 184 to confirm that the analysis region was located within the embryo tissue and not outside of it. Figure 4.2 shows the 2D ToF-SIMS ion maps of each ion, and the corresponding total ion counts are summarized in Table 4.6.

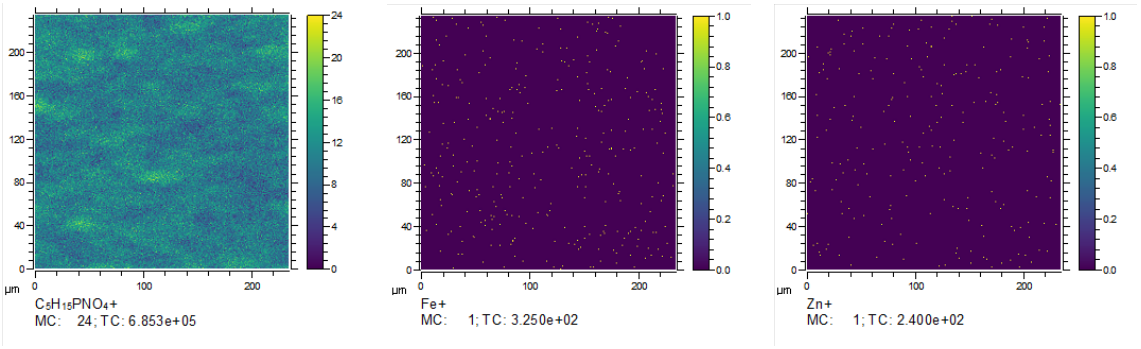

(a) $C_5H_{15}NO_4P^+$ **(b)** Fe^+ **(c)** Zn^+

Figure 4.2: ToF-SIMS ion maps of $C_5H_{15}NO_4P^+$, Fe^+ and Zn^+, in sample A1.

Table 4.6: ToF-SIMS ion counts detected in Sample A1.

No.	Ion	m/z	Counts
1	$C_5H_{15}NO_4P^+$	184.0883	867445
2	Zn^+	63.9300	240
3	Fe^+	55.9359	326

Table 4.6 shows a high signal intensity for the phosphocholine ion $C_5H_{15}NO_4P^+$ is 867445 counts, and significantly lower ion counts for Zn^+ (240 counts) and Fe^+ (326 counts). The high value for the phosphocholine fragment confirms tissue presence and proper targeting during analysis. In contrast, the low counts for zinc and iron reflect their baseline levels in the sample. As seen in Figure 4.2, their ion distributions are almost at noise level, indicating minimal metal signals in untreated samples. These values serve as a control for comparison with treated samples in later analyses.

Table 4.7 shows the signal intensities for $C_5H_{15}NO_4P^+$ and Zn^+, and Figure 4.3 presents the ion distributions of both phosphocholine and zinc, along with the corresponding mass spectrum.

Table 4.7: ToF-SIMS ion counts detected in Sample B1.

No.	Ion	m/z	Counts
1	$C_5H_{15}NO_4P^+$	184.2432	1025150
2	Zn^+	63.9178	418

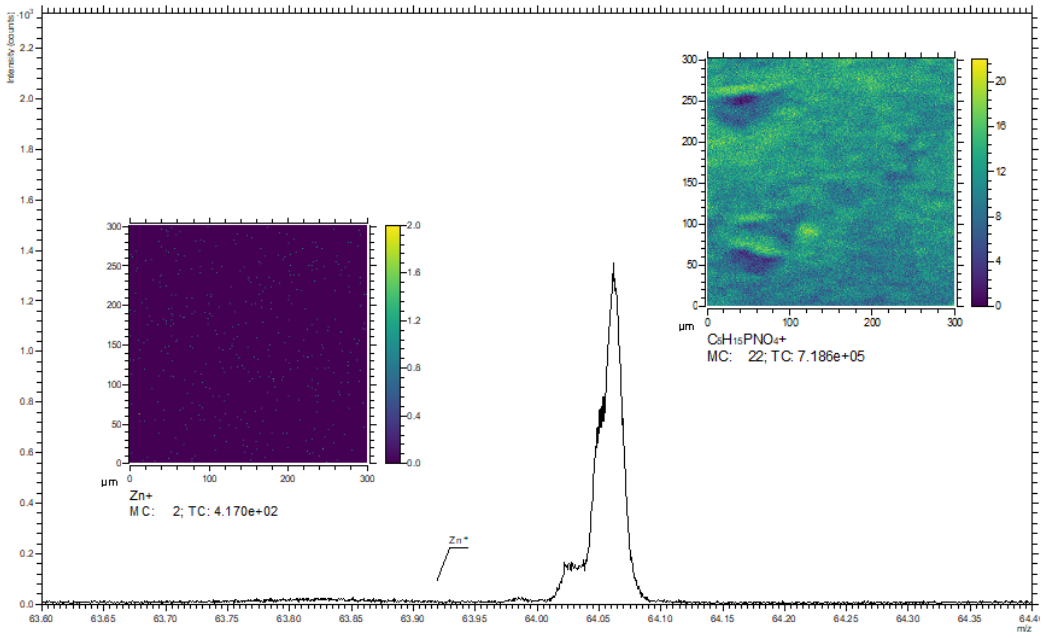

Figure 4.3: Mass spectrum and ion distributions of Zn^+ and $C_5H_{15}NO_4P^+$ in Sample B1

As illustrated in Table 4.7, the phosphocholine signal is high, while the zinc signal remains very low, even after treatment with a zinc standard solution. These values indicate that the analyzed region is indeed tissue; however, the penetration of zinc ions into the tissue appears to be ineffective. However, the Zn signal is nearly double the value observed in the reference sample, indicating a slight increase due to the treatment. This observation is further supported by Figure 4.3. The spectrum

includes a zoomed in view of the zinc ion signal around the m/z value of 63, where the zinc signal is nearly at noise level. This confirms that even after the addition of a zinc solution, the zinc ions are not effectively detected by ToF-SIMS. This may be attributed to either the limited penetration of zinc ions into the tissue matrix or the inherent limitations of ToF-SIMS in detecting zinc under these experimental conditions.

Sample A3 was treated with an iron standard solution at a concentration of 10 µg/mL. The corresponding ion counts and mass spectra are presented in Table 4.8 and Figure 4.4.

Table 4.8: ToF-SIMS ion counts detected in Sample A3.

No.	Ion	m/z	Counts
1	$C_5H_{15}NO_4P^+$	184.0269	4697108
2	Fe^+	55.9338	782

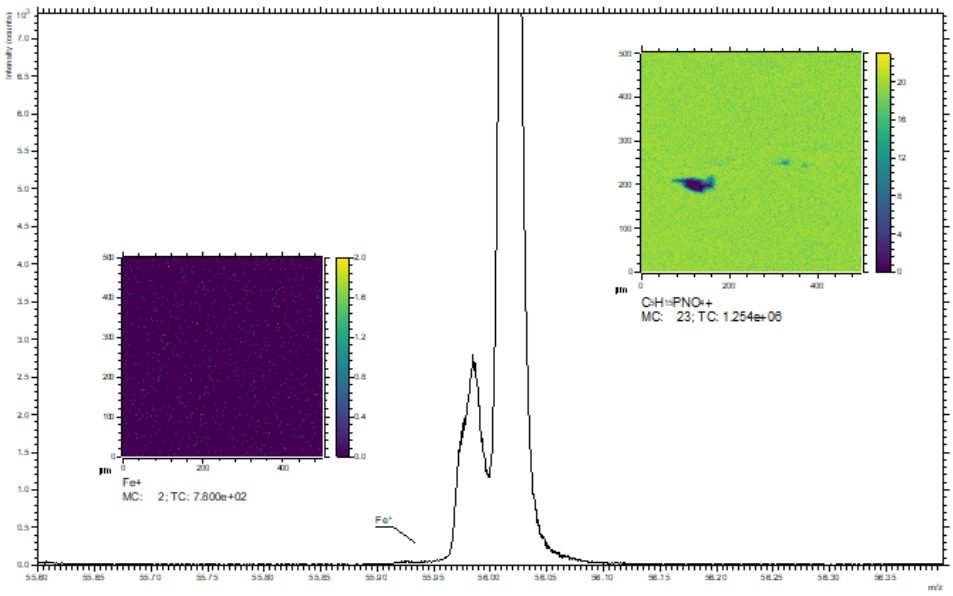

Figure 4.4: Mass spectrum and ion distributions of Fe^+ and $C_5H_{15}NO_4P^+$ in Sample A3

As shown in Table 4.8, the ion count for Fe^+ is approximately 782, while the signal for phosphocholine ($C_5H_{15}NO_4P^+$) remains high. The relatively low iron signal, even after the addition of an Fe standard solution to the embryo, suggests limited penetration of iron into the tissue or challenges in detecting Fe^+ ions in the tissue environment using ToF-SIMS. This observation is further supported by Figure 4.4, which shows the corresponding 2D ion distribution and a mass spectrum zoomed in around the Fe^+ m/z value of 56. In the spectrum, the iron signal appears close to the noise level, reinforcing the conclusion that Fe incorporation into the tissue is minimal or not easily detectable by this technique under these conditions.

As shown in Table 4.6 and Table 4.8, the signals for both iron (Fe^+) and zinc (Zn^+) ions were very low, even after the addition of standard solutions. To minimize the potential influence of surface contamination, sample A3 was sputtered using an argon gas cluster ion beam (GCIB) in ToF-SIMS. This sputtering process removes surface layers sequentially, allowing deeper regions of the sample to be analyzed. The ion counts and 2D ion distribution from the sputtered iron-treated sample (A3) are presented in Table 4.9 and Figure 4.5.

Table 4.9: ToF-SIMS ion counts detected in Sample A3 after sputtering with a gas cluster ion beam (GCIB).

No.	Ion	m/z	Counts
1	$C_5H_{15}NO_4P^+$	183.9289	521944
2	Fe^+	55.9337	1942

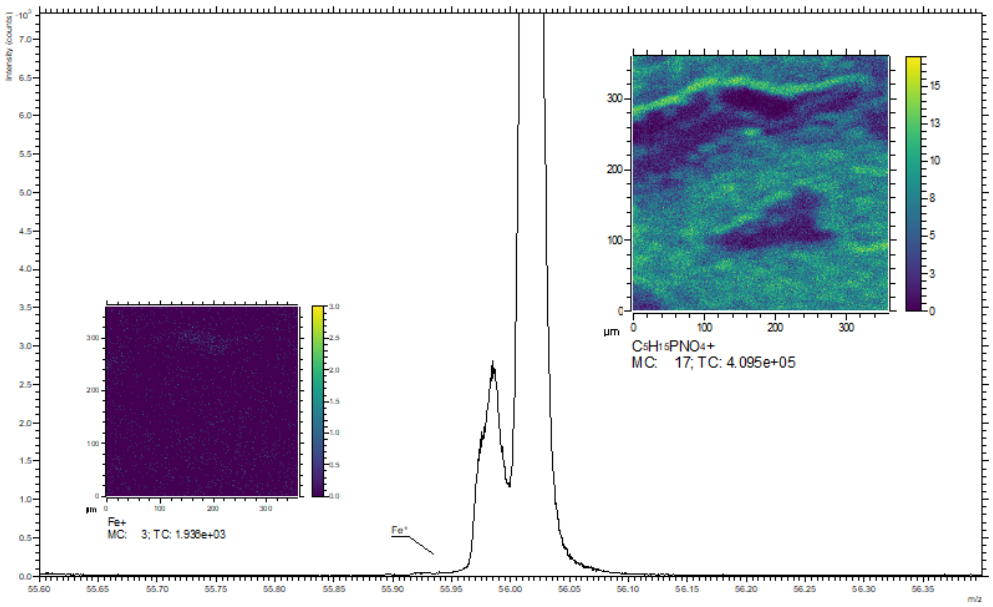

Figure 4.5: Mass spectrum and ion distributions of Fe^+ and $C_5H_{15}NO_4P^+$ in Sample A3 after sputtering with GCIB.

After sputtering, the signal intensity of the Fe^+ ion in sample A3 approximately doubled relative to the pre-sputtering measurement, as shown by the increased counts in Table 4.9. However, the total count remained low, around 1942. This is further supported by Figure 4.5, which illustrates the mass spectrum and ion distributions of both Fe^+ and phosphocholine. An overlay of $C_5H_{15}NO_4P^+$ and Fe^+ signals after sputtering is presented in Appendix A.3. The Fe^+ signal is still close to the noise level and does not appear as a clearly defined peak. This suggests that either electroporation was insufficient for effective penetration of iron ions into the tissue or that iron at this concentration is difficult to detect by ToF-SIMS under these conditions. Therefore, alternative sample preparation and analysis strategies should be explored, leading to the investigation of Sample Group B.

It is worth mentioning that additional replicates of the sample were also analyzed, but they exhibited the same pattern of low ion signals for both metals. As a result, these replicates were not included in the final results. Nevertheless, it is not possible to draw definitive conclusions regarding the detectability of iron or zinc ions based solely on these observations. Potential sources of error, such as instrument calibration deviations, variability in sample preparation steps, and inconsistencies in handling, may have influenced the outcome. Since the samples were prepared at different stages, these factors could contribute to the observed variation and signal suppression.

4.2.2 Group B

In this group, the embryos were incubated for 4 days. The main distinction between samples lies in the variation of treatment methods. In some cases, the Fe standard solution was mixed with DMSO only. Other samples were treated with a combination of electroporation and incubation following the addition of the standard. Additionally, some samples received only electroporation or only incubation, while others received no additional treatment. The specific treatment conditions for each sample are summarized in Table 3.4.

Sample B1 was treated with the Fe standard solution mixed with DMSO. The mass spectrum and ion distributions for Fe^+ and $C_5H_{15}NO_4P^+$ in Sample B1 are illustrated in Figure 4.6.

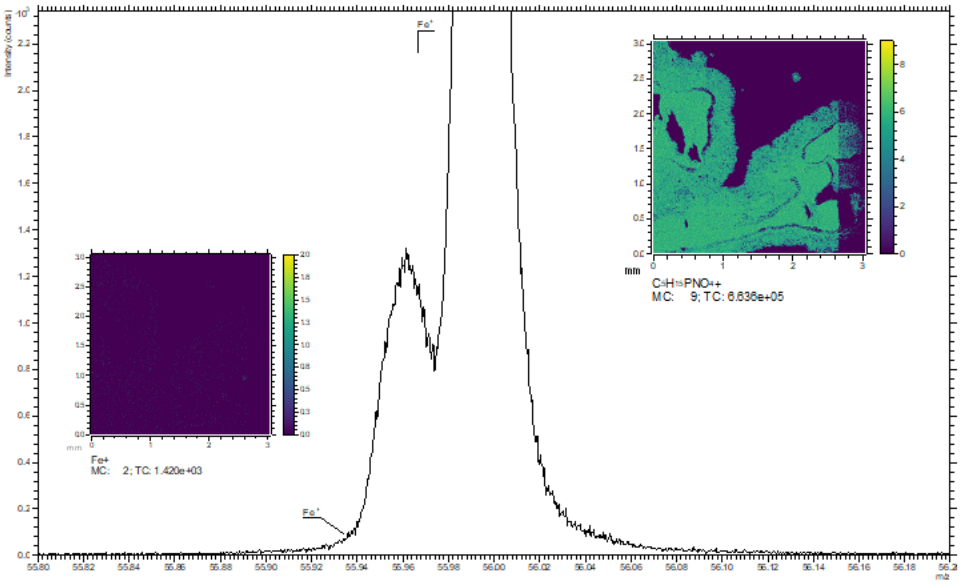

Figure 4.6: Mass spectrum and ion distributions of Fe^+ and $C_5H_{15}NO_4P^+$ in Sample B1.

Sample A2 in this group was treated with the Fe and DMSO mixture and subjected to electroporation. After treatment, it was incubated at 37 °C for 30 minutes. The ion counts for this sample are shown in Figure 4.7.

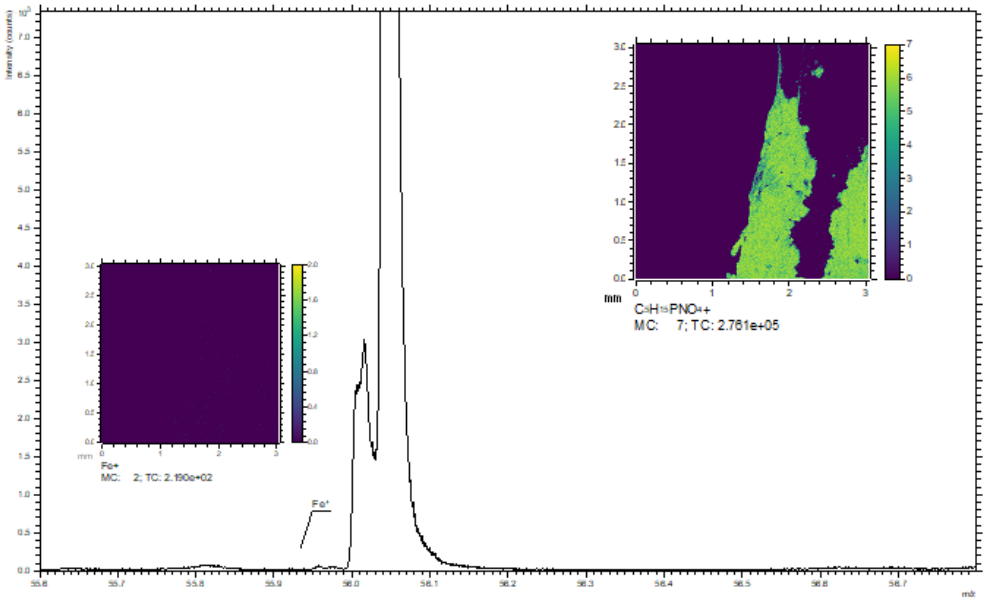

Figure 4.7: Mass spectrum and ion distributions of Fe^+ and $C_5H_{15}NO_4P^+$ in Sample A2.

Sample A3 was treated in the same way as Sample A2 but was not incubated after treatment. The mass spectrum and ion distributions for iron and the phosphocholine cation are shown in Figure 4.8.

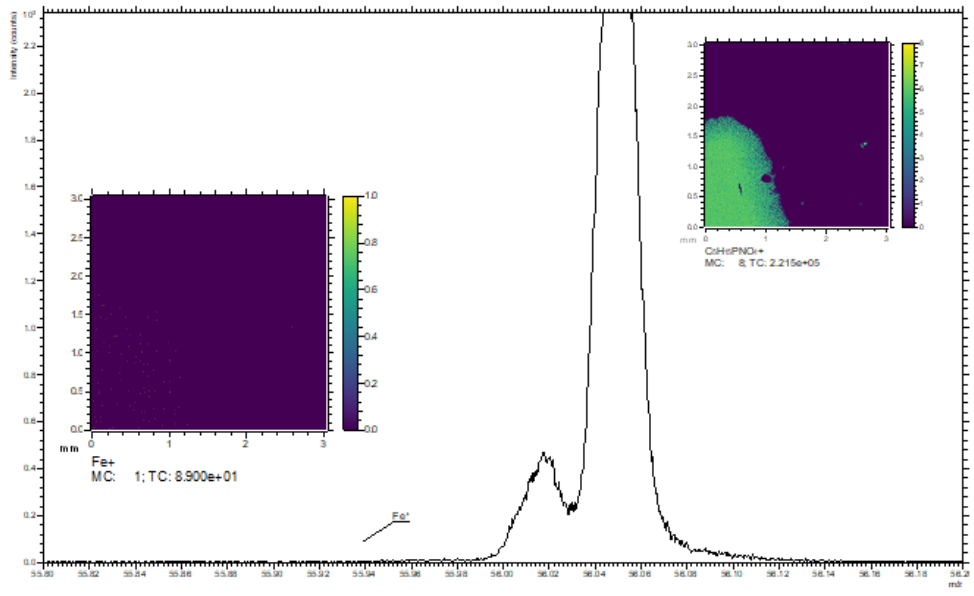

Figure 4.8: Mass spectrum and ion distributions of Fe^+ and $C_5H_{15}NO_4P^+$ in Sample A3.

Sample A4 was treated with the Fe standard solution, electroporated, and also incubated for 30 minutes after treatment. The mass spectrum and ion distributions for Fe^+ and $C_5H_{15}NO_4P^+$ in Sample A4 are illustrated in Figure 4.9.

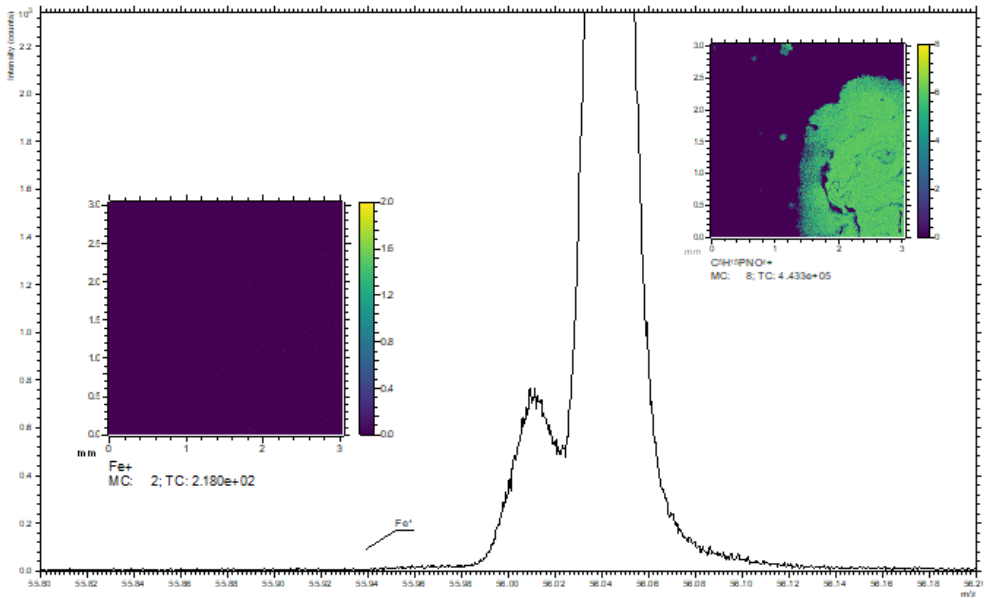

Figure 4.9: Mass spectrum and ion distributions of Fe^+ and $C_5H_{15}NO_4P^+$ in Sample A4.

A summary of Fe^+ and $C_5H_{15}PNO_4^+$ ion counts across Group B samples with different treatment methods is shown in Table A.2 in Appendix. As the samples were analyzed in a 2D setting, the analysis areas differed between each sample. To enable a more accurate comparison, the Fe^+ to $C_5H_{15}PNO_4^+$ ion ratio was used. Column four in Table 4.10 shows the ratio of Fe^+ to $C_5H_{15}PNO_4^+$ cation.

Table 4.10: Summary of Fe^+ counts and $Fe^+/C_5H_{15}PNO_4{}^+$ ratios across Group B samples with different treatment methods.

Sample	**Treatment Method**	**Fe^+ (cts)**	**$Fe^+/C_5H_{15}PNO_4{}^+$**
B1	Fe + DMSO	1426	0.000943
A2	Fe + DMSO, electro + incub	219	0.000306
A3	Fe + DMSO, electro	89	0.000152
A4	Fe, electro + incub	218	0.000191

Sample B1, which was treated with Fe and DMSO only, showed the highest iron/phosphocholine signal. However, overall Fe^+ ion signals across all samples were relatively low, nearly at the noise level, with no clearly defined peaks, as also confirmed by the mass spectra and ion distributions shown in Figures 4.6–4.9. Despite the low signal, comparison of treatment methods within this group suggests that DMSO may enhance Fe ion penetration. The Fe^+ signal in B1 was approximately double that of sample A3 (782 counts) from Group A, which was treated with Fe solution without DMSO but underwent electroporation. This observation may support the hypothesis presented in the theory section that DMSO facilitates metal ion uptake.

However, samples A2 and A3, which were treated with Fe and DMSO but also

underwent electroporation (with or without incubation), showed very low Fe signals close to the noise level. This suggests that the interaction between DMSO and additional treatment steps, such as electroporation or incubation, may influence ion uptake negatively. Sample A4, which was electroporated and incubated after Fe treatment without DMSO, showed a Fe^+ signal of 218 counts, comparable to A2. It is worth noting that overall ion counts were low across all samples; therefore, no definitive or representative conclusion can be drawn. These interpretations remain limited and are based on a small number of analyzed samples. The $Fe^+/C_5H_{15}PNO_4{}^+$ ratios for all samples in Group B are visualized as a bar chart in Figure 4.10.

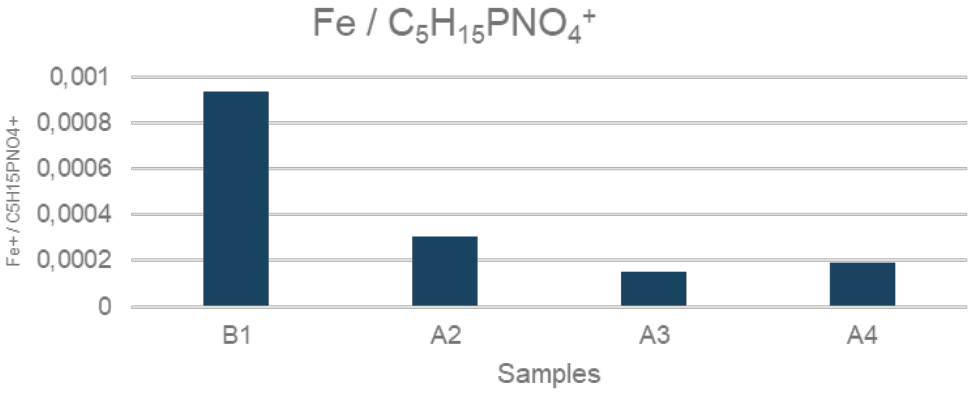

Figure 4.10: Summary of Fe ion signals across samples in Group B

As shown in Table 4.10, different sample treatment strategies did not significantly affect the Fe^+ ion signal counts. Therefore, alternative strategies were explored, including a comparison of metal treatment timing and the introduction of a new metal element, copper. This led to the formation of Sample Group C.

4.2.3 Group C

In this group, samples were treated with a copper standard solution. The treatment timepoint varied between samples to determine the most optimal conditions for the TOF-SIMS analysis of metal elements in tissue samples. These samples were first analyzed using 2D large-area analysis to identify the sample regions. Selected regions were then further analyzed in both 2D and 3D modes after sputtering, to ensure the removal of surface contamination. Each sample had three replicates, in which the ion signals of two copper isotopes, ^{63}Cu and ^{65}Cu, as well as phosphocholine cation ($C_5H_{15}PNO_4{}^+$) were recorded. The average values and corresponding errors from the three replicates are reported for each sample type.

Sample B1 was treated with the copper standard solution before freeze-drying and analyzed using the 2D large area setting. Ion counts of two copper isotopes, ^{63}Cu and ^{65}Cu, as well as the phosphocholine cation ($C_5H_{15}PNO_4^+$), were recorded for three replicates. The initial values, averages, and corresponding standard deviations of these ion counts from the three replicates are presented in Table A.3 in the appendix.

Table 4.11 illustrates the ratio of copper isotope signals to the phosphocholine ion signal. Ion distributions for all three ions in replicate 1 are shown in Figure 4.11, while the mass spectra are displayed only for the copper isotopes.

Ion	**$^{63}Cu^+$/ $C_5H_{15}PNO_4^+$**	**$^{65}Cu^+$ /$C_5H_{15}PNO_4^+$**	**$C_5H_{15}PNO_4^+$**
	0.057820	0.01710	1743084

Table 4.11: Ratio of copper isotope to the phosphocholine cation from three TOF-SIMS replicates of Sample B1.

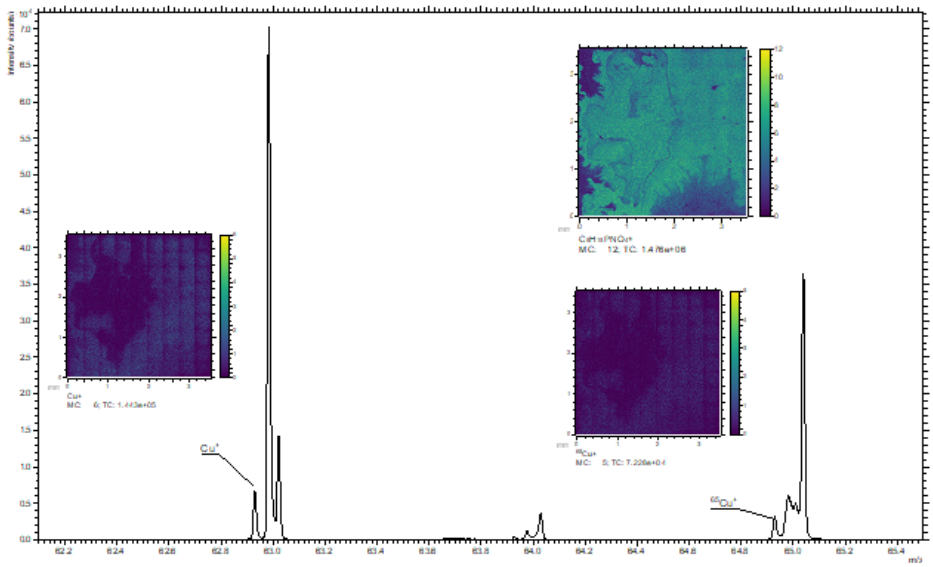

Figure 4.11: Mass spectrum and ion distributions of $^{63}Cu^+$, $^{65}Cu^+$, and $C_5H_{15}NO_4P^+$ in replicate 1 of Sample B1 from Group C. The mass spectra are shown for the copper isotopes, while ion distributions are presented for all three ions.

Sample A1 in this group was treated with the copper standard solution after freeze-drying, prior to TOF-SIMS analysis. Ion counts of two copper isotopes, ^{63}Cu and ^{65}Cu, as well as the phosphocholine cation ($C_5H_{15}PNO_4^+$), were recorded for three replicates. The initial values, averages, and corresponding standard deviations of these ion counts from the three replicates are presented in Table A.4 in the appendix.

Table 4.12 illustrates the ratio of copper isotope signals to the phosphocholine ion signal. Ion distributions for all three ions in replicate 1 are shown in Figure 4.12, while the mass spectra are displayed only for the copper isotopes.

Ion	**$^{63}Cu^+$/ $C_5H_{15}PNO_4^+$**	**$^{65}Cu^+$ /$C_5H_{15}PNO_4^+$**	**$C_5H_{15}PNO_4^+$**
	0.075914	0.026791	1952966

Table 4.12: Ratio of copper isotope to the phosphocholine cation from three TOF-SIMS replicates of Sample A1.

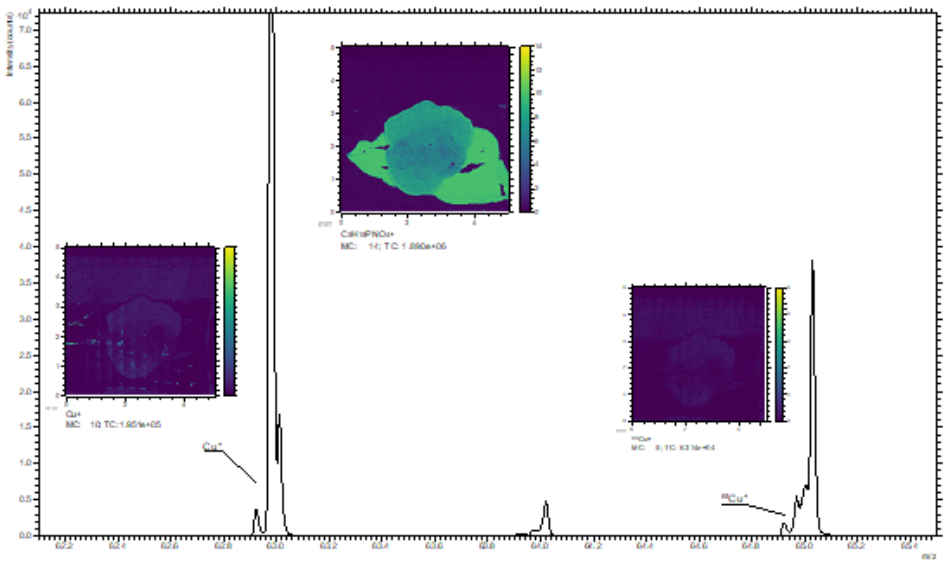

Figure 4.12: Mass spectrum and ion distributions of ^{63}Cu, ^{65}Cu and ($C_5H_{15}PNO_4^+$) in replicate 1 of Sample A1 from group C

Two different replicates of untreated chicken embryo samples were analyzed using ToF-SIMS. Both samples were prepared according to the general procedure described in Section 3.1.2.3 and were then analyzed using the 2D large area setting to locate the embryo region. Subsequently, specific regions of interest were selected, where surface layers were sputtered with a GCIB of argon gas to remove potential surface contamination and to study thin surface layers of the sample for depth profiling.

Ion counts for $^{63}Cu^+$, $^{65}Cu^+$, $C_5H_{15}PNO_4^+$, and silicon (Si), which corresponds to the underlying glass slide on which the embryo was thawed, were recorded under all settings. The initial ion signals for both samples are presented in Table A.5 in the appendix, and the ratios of $^{65}Cu^+$ and $^{63}Cu^+$ to phosphocholine are presented in Table 4.13 for both samples.

Sample	**$^{63}Cu^+$/ $C_5H_{15}PNO_4^+$**	**$^{65}Cu^+$ /$C_5H_{15}PNO_4^+$**	**$C_5H_{15}PNO_4^+$**
A4	0.0375	0.0283	547662
A2	0.0263	0.0073	276052

Table 4.13: Ratio of copper isotope to the phosphocholine cation for untreated samples Sample A4 and A2.

As illustrated in the table, the ratio of copper isotopes to phosphocholine is reasonably high and beyond the noise level, which demonstrates that copper is detectable by ToF-SIMS even in untreated samples.

Figures 4.13 and 4.14 show the mass spectra for copper isotopes and the 2D ion distributions of $^{63}Cu^+$, $^{65}Cu^+$, and $C_5H_{15}PNO_4^+$ for samples A4 and A2, respectively.

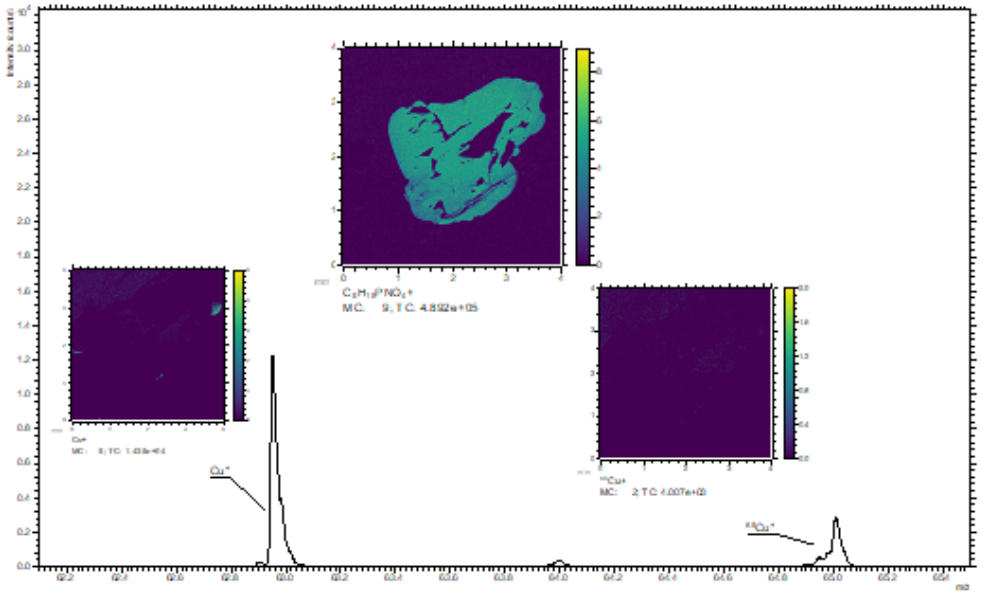

Figure 4.13: Mass spectrum and ion distributions of ^{63}Cu, ^{65}Cu and $C_5H_{15}PNO_4^+$ in Sample A4 from group C

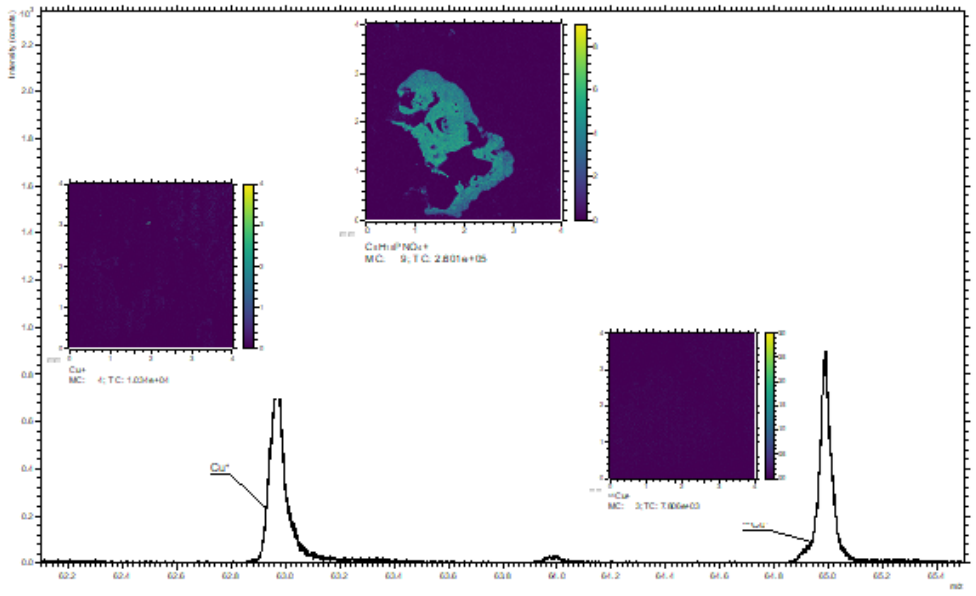

Figure 4.14: Mass spectrum and ion distributions of ^{63}Cu, ^{65}Cu and $C_5H_{15}PNO_4^+$ in Sample A2 from group C

Specific regions of Sample A4 and A2 were analyzed in 3D mode, and one representative region for each sample are illustrated in Figure 4.15.

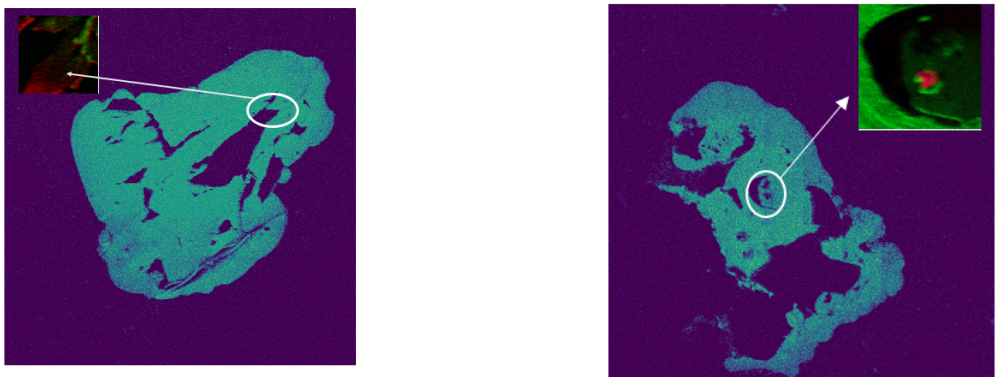

(a) Sputtered region of sample A4 **(b)** Sputtered region of sample A2

Figure 4.15: Sputtered regions of samples A4 and A2.

The ion distributions of $^{63}Cu^+$, $^{65}Cu^+$, $C_5H_{15}PNO_4^+$, and Si within these regions are shown in the figure 4.16. Panels (a), (b), and (c) correspond to $^{63}Cu^+$, $^{65}Cu^+$, and $C_5H_{15}PNO_4^+$, respectively; panel (d) shows the distribution of Si. Panels (e) and (f) display the overlay of $^{63}Cu^+$ with $C_5H_{15}PNO_4^+$ and with Si, respectively.

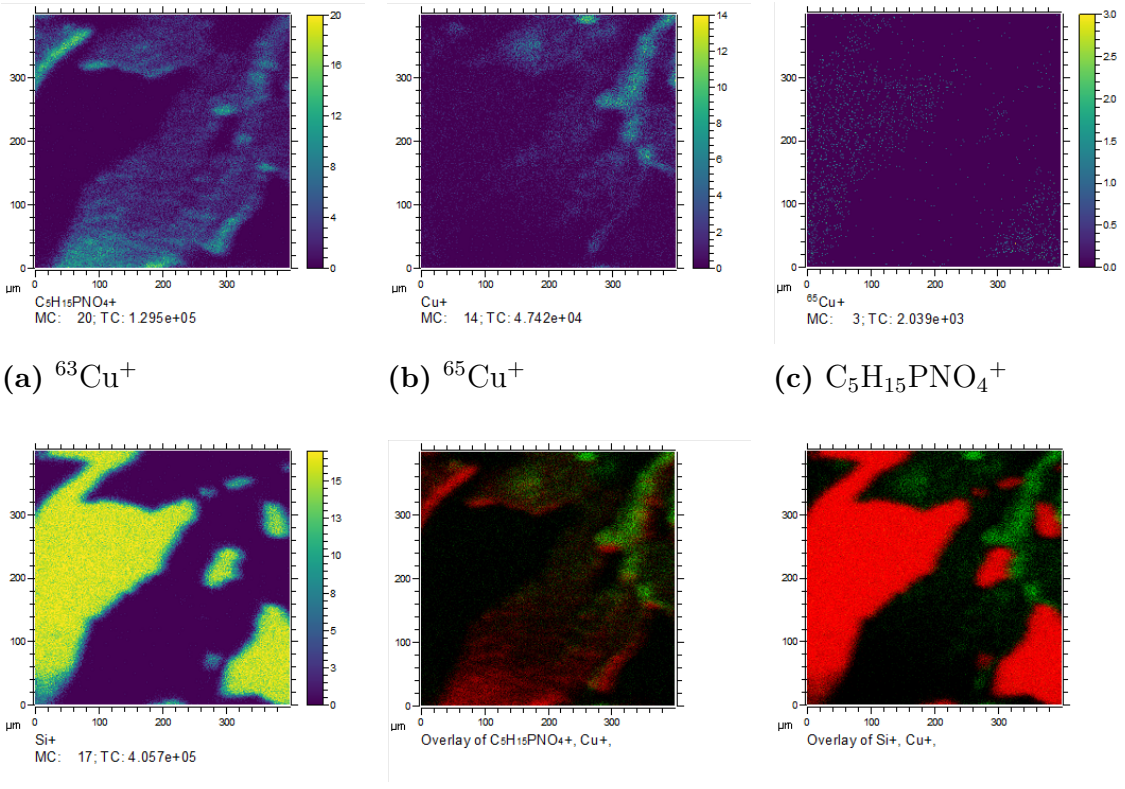

(a) $^{63}Cu^+$ **(b)** $^{65}Cu^+$ **(c)** $C_5H_{15}PNO_4{}^+$

(d) Si^+ **(e)** Overlay of c and b **(f)** Overlay of d and b

Figure 4.16: TOF-SIMS ion distributions of $^{63}Cu^+$, $^{65}Cu^+$, $C_5H_{15}PNO_4{}^+$, Si^+ and overlay of $^{63}Cu^+$ with $C_5H_{15}PNO_4^+$ and with Si in Sample A4.

The lack of overlap between $^{63}Cu^+$ and Si in panel (e) of Figure 4.16 suggests that the copper signal does not originate from the glass slide on which the embryo

was thawed. In contrast, the clear overlap between $^{63}Cu^+$ and phosphocholine in panel (f) indicates that the copper signal is associated with the tissue region. This supports the conclusion that $^{63}Cu^+$ is detectable by ToF-SIMS in a biological tissue environment under the conditions used.

For sample A2, the ion signals and the corresponding overlays of the signals are shown in Figure 4.17.

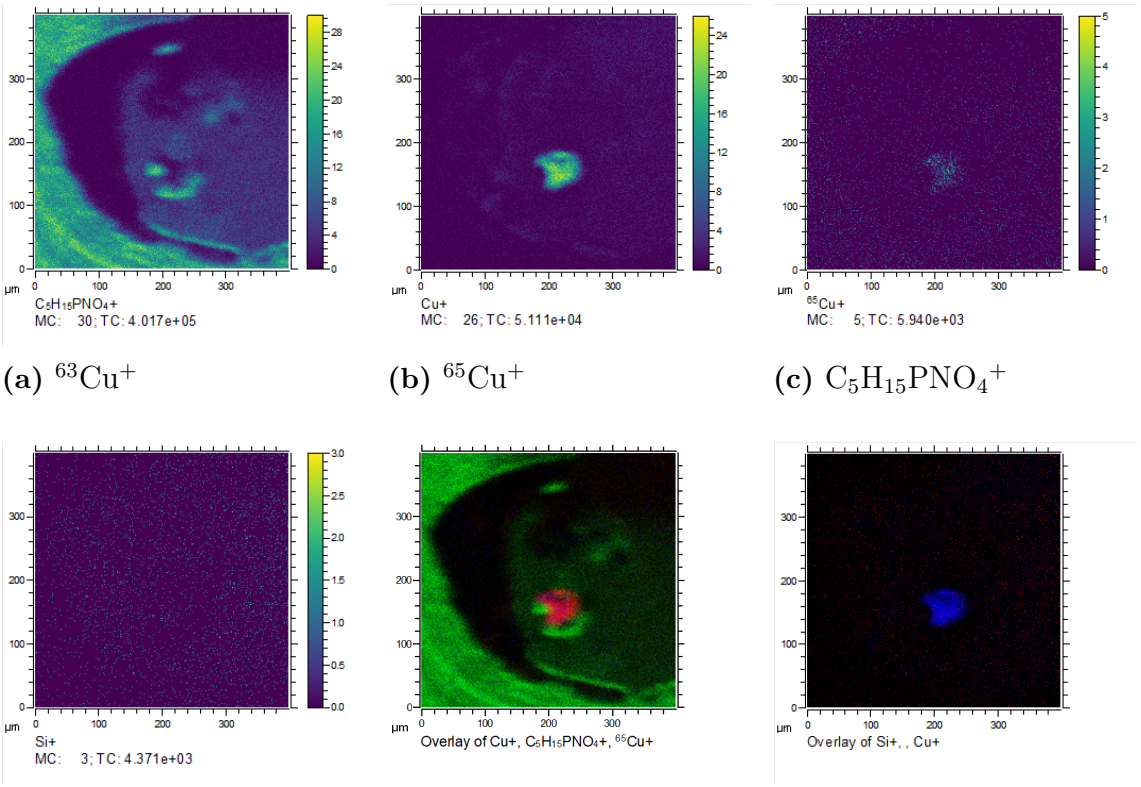

(a) $^{63}Cu^+$ **(b)** $^{65}Cu^+$ **(c)** $C_5H_{15}PNO_4{}^+$

(d) Si **(e)** Overlay of a, b and c **(f)** Overlay of a and d

Figure 4.17: TOF-SIMS ion distributions of $^{63}Cu^+$, $^{65}Cu^+$, $C_5H_{15}PNO_4{}^+$, Si^+ and overlay of $^{63}Cu^+$ with $C_5H_{15}PNO_4^+$ and with Si in Sample A2.

For sample A2, as shown in Figure 4.17d, the Si signal is almost at the noise level, and there is no clear overlay between Si and $^{63}Cu^+$, which might be due to the low Si signal intensity. The overlay between $^{63}Cu^+$, $^{65}Cu^+$, and phosphocholine Figure 4.17e is not very strong but does show some partial overlap. This suggests that the copper signal partly originates from the embryo tissue; however, it remains unclear whether there is any overlap with the Si signal.

From both Figure 4.16 and Figure 4.17, the observed overlap between $^{63}Cu^+$ and phosphocholine signals suggests that the copper originates, at least in part, from the embryo tissue rather than the underlying glass slide. This supports the conclusion that $^{63}Cu^+$ is detectable by ToF-SIMS in a biological tissue environment.
To verify the reliability of the copper ion signal, MCR analysis was performed using SurfaceLab software on sputtered regions of both untreated samples. This method

was employed to extract the pure spectral contributions of $^{63}Cu^+$ and $C_5H_{15}PNO_4^+$ from the measured mass spectra and ion distribution images. The analysis was conducted using 10 factors. The principle of MCR is that the data is decomposed into several factors, where each factor has a loading plot and a corresponding ion distribution pattern. The most intense peak in the loading plot corresponds to the most prominent element in the sample.

For sample A4, the loading plots and ion distributions corresponding to the characteristic copper and phosphocholine peaks are shown in Figures 4.18 and 4.19, respectively.

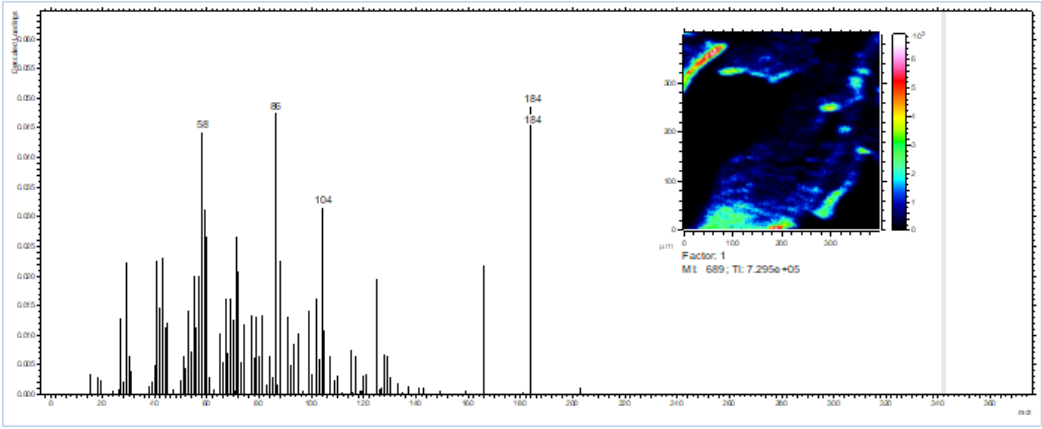

Figure 4.18: MCR analysis of sample A4, factor 1 loading plot and ion distribution

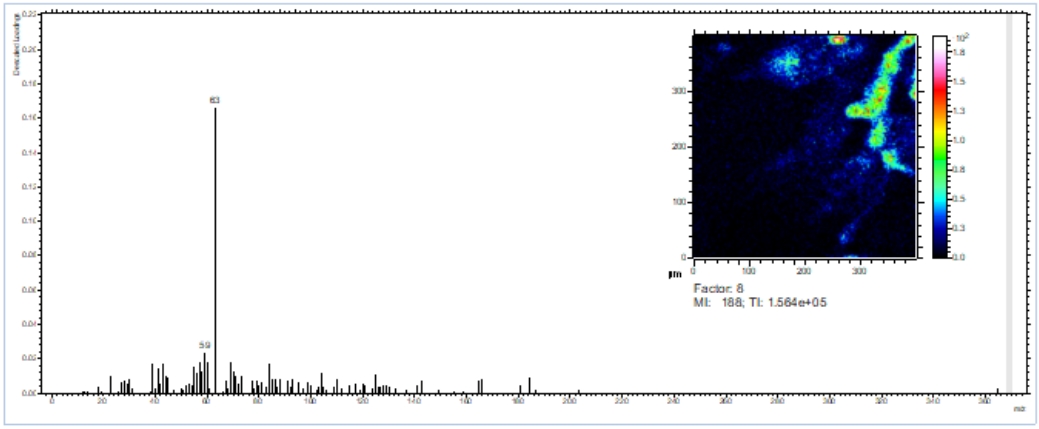

Figure 4.19: MCR analysis of sample A4, factor 8 loading plot and iondistribution

Figure 4.18 corresponds to factor 1 of the MCR analysis, where the highest peak in the loading plot shows an m/z value of 184, which corresponds to the phosphocholine cation $C_5H_{15}PNO_4^+$. While factor 8 of the analysis shows a dominant signal at m/z 63, corresponding to $^{63}Cu^+$. This finding further supports the conclusion that the signals for both Cu^+ and $C_5H_{15}PNO_4^+$ in the ToF-SIMS data are chemically meaningful and that the copper signals originate from the embryo region.

Figures 4.18 and 4.19 show two factors from the MCR analysis for sample A2.

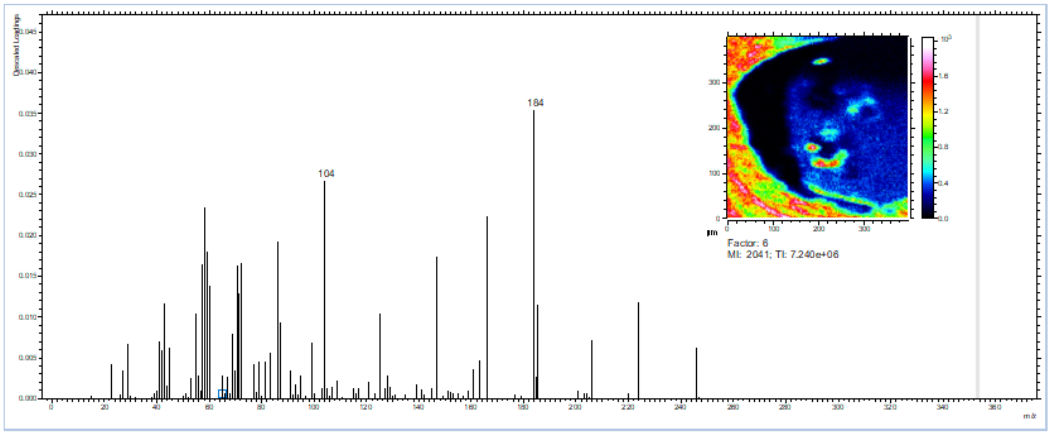

Figure 4.20: MCR analysis of sample A2, factor 6 loading plot and ion distribution

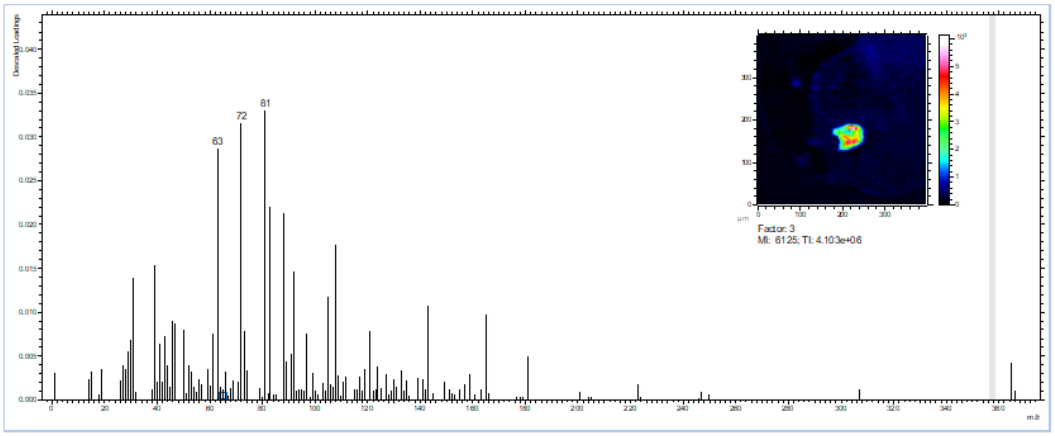

Figure 4.21: MCR analysis of sample A2, factor 3 loading plot and ion distribution

Figure 4.18, corresponding factor 6 of the MCR analysis, displays the loading plot and ion distribution for phosphocholine ($C_5H_{15}PNO_4^+$), while factor 3 shows the loading plot with the highest peak at m/z 63, reflecting copper ($^{63}Cu^+$). However, there are also other dominant peaks at m/z 72 and 81, which may be associated with organic fragments corresponding to possible contamination or unidentified species. Further research is needed to confirm their chemical identity.

In general, factors 8 and 1 in sample A4 and factors 6 and 3 in sample A2 confirm the presence of copper signals from the chicken embryo region and demonstrate the capability of ToF-SIMS to detect copper under the experimental conditions applied. However, it is important to note that this conclusion is based on a small number of samples and limited data. Therefore, while these results are promising, they are not sufficient to draw definitive conclusions regarding the detectability and localization of copper in tissue using ToF-SIMS. Further studies with larger sample sizes and additional controls are necessary to confirm these findings.

When comparing metal element detection in cancer cells and chicken embryo models, the isotopic fraction observed is dependent on the matrix in which the sample is found. The matrices differed between the two sample types, and due to challenges in detecting the signal of specific metals using ToF-SIMS, the metal elements studied within these matrices were also different. As a result, a direct comparison of these two matrices was not possible in this project, making it difficult to draw definitive conclusions regarding the matrix effect on the isotopic fraction of metal elements in these samples. Future research should include larger sample sizes and targeted investigations of the matrix effect to strengthen and validate these observations.

5
Conclusion

This project demonstrated clear isotopic fractionation trends in cancer cells. Zinc exhibited significant depletion in the heavier isotope in both treated and untreated cancer cells, which corresponds well to previous findings in the literature describing zinc isotope behavior in cancer cells. For calcium, a strong connection between isotopic fractionation and bone marrow cancer (myeloma) has been described in the litterature. Similarly, in this study, breast cancer cells showed strong enrichment in the heavier calcium isotope in both conditins. Iron and magnesium showed depletion in heavier isotopes in untreated cells, however, treated cells exhibited different trends. Unlike zinc, a direct correlation between iron and magnesium isotopic fractionation and cancer has not been clearly established in the literature, although their links to other diseases, such as diabetes and metabolic disorders, have been reported.

However, it is important to mention that only six technical replicates per sample were analyzed, which limits the representativeness and robustness of these conclusions. Potential sources of error during sample preparation and analysis could also have influenced the results.

In the chicken embryo tissue experiments, zinc and iron at 10µg/mL were not detectable by ToF-SIMS under the conditions used, despite sputtering slightly enhancing detection. Overall, their signal remained low. Furthermore, DMSO may enhance cell permeability, however, its interaction with electroporation in this study remains unclear. The uncertainty surrounding the DMSO effect may be due to variations in treatment methods, and further research with additional replicates is necessary to draw more representative and reliable conclusions. Both $^{63}Cu^{+}$ and $^{65}Cu^{+}$ ions were consistently detectable in both treated and untreated samples, indicating that copper is readily detectable even at low concentrations. This supports the conclusion that ToF-SIMS is a matrix-dependent, semi-quantitative technique that can provide relative quantification compared to a standard, but does not yield absolute concentration measurements.

Overall, while this study provides important preliminary insights into isotopic fractionation patterns in cancer cells and chicken embryo tissues, further experiments with larger sample sizes and refined protocols are needed to confirm these findings and improve their diagnostic relevance.

Bibliography

1. Bray F, Laversanne M, Sung H, Ferlay J, Siegel RL, Soerjomataram I, and Jemal A. Global cancer statistics 2022: GLOBOCAN estimates of incidence and mortality worldwide for 36 cancers in 185 countries. CA: A Cancer Journal for Clinicians. 74:229–63. DOI: https://doi.org/10.3322/caac.21834
2. American Cancer Society. Cancer Facts & Figures 2025. [Internet]. [cited 2025 Aug 3]. Atlanta, 2025. Available from: https://www.cancer.org/content/dam/cancer-org/research/cancer-facts-and-statistics/annual-cancer-facts-and-figures/2025/2025-cancer-facts-and-figures-acs.pdf
3. Henry NL and Hayes DF. Cancer biomarkers. Molecular oncology 2012; 6:140–6. DOI: 10.1016/j.molonc.2012.01.010. Available from: https://doi.org/10.1016/j.molonc.2012.01.010
4. Larner F. Can we use high precision metal isotope analysis to improve our understanding of cancer? Analytical and Bioanalytical Chemistry 2016; 408:345–9. DOI: 10.1007/s00216-015-9201-5. Available from: https://doi.org/10.1007/s00216-015-9201-5
5. Liberti MV and Locasale JW. The Warburg Effect: How Does it Benefit Cancer Cells? Trends in Biochemical Sciences 2016; 41:211–8. DOI: 10.1016/j.tibs.2015.12.001
6. Larner F, Woodley LN, Shousha S, Moyes A, Humphreys-Williams E, Strekopytov S, Halliday AN, Rehkämper M, and Coombes RC. Zinc isotopic compositions of breast cancer tissue. Metallomics 2015; 7:112–7. DOI: 10.1039/c4mt00260a. eprint: 2014Dec9
7. Zoroddu MA, Aaseth J, Crisponi G, Medici S, Peana M, and Nurchi VM. The essential metals for humans: a brief overview. Journal of Inorganic Biochemistry 2019; 195:120–9. DOI: 10.1016/j.jinorgbio.2019.03.013. Available from: https://www.sciencedirect.com/science/article/pii/S0162013418306846
8. Encyclopaedia Britannica. Elemental and Isotopic Abundances. https://www.britannica.com/science/isotope/Elemental-and-isotopic-abundances. Accessed May 18, 2025. 2024
9. Rahaman W. Non-traditional stable metal and metalloid isotopes and their potential applications in earth, ocean, and environmental sciences. Geosystems and Geoenvironment 2024; 3:100307. DOI: 10.1016/j.geogeo.2024.100307. Available from: https://www.sciencedirect.com/science/article/pii/S2772883824000578

10. National Cancer Institute. What Is Cancer? Accessed: 2024-10-18. 2021. Available from: https://www.cancer.gov/about-cancer/understanding/what-is-cancer
11. Manaprasertsak A, Kazi JU, Hagerling C, Pienta KJ, Malmberg P, and Hammarlund EU. Alterations of the chemical profile of cholesterol in cancer tissue as traced with ToF-SIMS. Analyst 2024; 149(21):5344–52. DOI: 10.1039/D4AN01050G
12. Zhao Z, Li T, Sun L, Yuan Y, and Zhu Y. Potential mechanisms of cancer-associated fibroblasts in therapeutic resistance. Biomedicine Pharmacotherapy 2023; 166:115425. DOI: https://doi.org/10.1016/j.biopha.2023.115425. Available from: https://www.sciencedirect.com/science/article/pii/S0753332223012234
13. Britannica. Pyruvic Acid. 2023 Jan 26. Available from: https://www.britannica.com/science/pyruvic-acid [Accessed on: 2025 Jan 21]
14. Vander Heiden MG, Cantley LC, and Thompson CB. Understanding the Warburg effect: the metabolic requirements of cell proliferation. Science 2009; 324:1029–33. DOI: 10.1126/science.1160809
15. Britannica. Adenosine Triphosphate. 2023 Jan 26. Available from: https://www.britannica.com/science/adenosine-triphosphate [Accessed on: 2025 Jan 21]
16. Institutet K. Positron Emission Tomography (PET). 2023. Available from: https://ki.se/en/research/research-infrastructure-and-environments/core-facilities-for-research/brain-molecular-imaging-centre-bmic/positron-emission-tomography-pet [Accessed on: 2025 Jan 21]
17. Sabatini DM. Corresponding Author: Whitehead Institute for Biomedical Research. Whitehead Institute for Biomedical Research, Nine Cambridge Center, Cambridge, MA 02142. Received: July 19, 2012; Revision Received: August 21, 2012; Accepted: August 21, 2012; Phone: 617-258-6407; Fax: 617-452-3566; E-mail: sabatini@wi.mit.edu. 2012
18. Gross JH. Introduction. *Mass Spectrometry*. Springer, Cham, 2017. DOI: 10.1007/978-3-319-54398-7_2
19. Gross JH. Mass Spectrometry: A Textbook. Cham: Springer International Publishing, 2017 :29–84. DOI: 10.1007/978-3-319-54398-7_2
20. Ligon WV. Organic Mass Spectrometry. *Encyclopedia of Materials: Science and Technology*. Ed. by Buschow KHJ, Cahn RW, Flemings MC, Ilschner B, Kramer EJ, Mahajan S, and Veyssière P. Elsevier, 2001 :6552–5. DOI: 10.1016/B0-08-043152-6/01158-X
21. Gross JH. Instrumentation. *Mass Spectrometry*. Springer, Cham, 2017. DOI: 10.1007/978-3-319-54398-7_4
22. Gates P. Ion Detectors. http://www.chm.bris.ac.uk/ms/detectors.xhtml. Accessed: 15-04-2020
23. Welker RW. Chapter 4 - Size Analysis and Identification of Particles. *Developments in Surface Contamination and Cleaning*. Ed. by Kohli R and Mittal K. Oxford: William Andrew Publishing, 2012 :179–213. DOI:

10.1016/B978-1-4377-7883-0.00004-3. Available from: https://www.sciencedirect.com/science/article/pii/B9781437778830000043

24. Shard AG, Spencer SJ, Smith SA, Havelund R, and Gilmore IS. The matrix effect in organic secondary ion mass spectrometry. International Journal of Mass Spectrometry 2015; 377. Special Issue: MS 1960 to Now:599–609. DOI: 10.1016/j.ijms.2014.06.027. Available from: https://www.sciencedirect.com/science/article/pii/S138738061400253X
25. Juan A TR de. Multivariate Curve Resolution: 50 years addressing the mixture analysis problem – A review. Anal Chim Acta 2021; 1145:59–78. DOI: 10.1016/j.aca.2020.10.051
26. Raso J and Álvarez I. Pulsed Electric Field Processing: Cold Pasteurization. *Innovative Food Processing Technologies*. Ed. by Knoerzer K and Muthukumarappan K. Elsevier, 2016 :288–96. DOI: 10.1016/B978-0-12-815781-7.03103-6. Available from: https://www.sciencedirect.com/science/article/pii/B9780128157817031036
27. Merck. Phosphate Buffered Saline, pH 7.4, liquid, sterile-filtered, suitable for cell culture. Accessed 2025 May 30. 2025. Available from: https://www.sigmaaldrich.com/US/en/product/sial/806552
28. Sigma-Aldrich, Merck. Paraformaldehyde, powder, 95%. Accessed 2025 May 30. 2025. Available from: https://www.sigmaaldrich.com/SE/en/product/sial/158127
29. Kim SO, Kim J, Okajima T, and Cho NJ. Mechanical properties of paraformaldehyde-treated individual cells investigated by atomic force microscopy and scanning ion conductance microscopy. Nano Converg 2017; 4:5. DOI: 10.1186/s40580-017-0099-9. Available from: https://doi.org/10.1186/s40580-017-0099-9
30. Royal Society of Chemistry. ChemSpider: Dimethyl sulfoxide (CSID: 659). Accessed 2025 May 30. 2025. Available from: https://www.chemspider.com/Chemical-Structure.659.html
31. Tunçer Çağlayan S and Gurbanov R. Modulation of bacterial membranes and cellular macromolecules by dimethyl sulfoxide: A dose-dependent study providing novel insights. Int J Biol Macromol 2024; 267:131581. DOI: 10.1016/j.ijbiomac.2024.131581. Available from: https://www.sciencedirect.com/science/article/pii/S0141813024023869
32. Zhang Y, Jen FEC, Fox KL, Edwards JL, and Jennings MP. The biosynthesis and role of phosphorylcholine in pathogenic and nonpathogenic bacteria. Trends Microbiol 2023; 31:692–706. DOI: 10.1016/j.tim.2023.01.006. Available from: https://www.sciencedirect.com/science/article/pii/S0966842X23000240
33. National Center for Biotechnology Information. PubChem Compound Summary for CID 1014, N,N,N-trimethyl-2-(phosphonooxy)ethanaminium. Accessed 2025 May 30. 2025. Available from: https://pubchem.ncbi.nlm.nih.gov/compound/N_N_N-trimethyl-2-_phosphonooxy_ethanaminium

A

Appendix 1

A.1 Summary of Isotopic Fractionation Values in Cancer Cell Samples

Table A.1: Summary of Isotopic Composition and Fractionation in Cell Samples for Zn, Ca, Fe, and Mg

Element	Sample Group	Isotope Ratio	δ Value (‰)
Zn	Cell	0.7094	–223
Zn	Cell + Zn	0.5260	–424
Ca	Cell	0.05004	+1186
Ca	Cell + Ca	0.08083	+2532
Fe	Cell	3.9202	–789
Fe	Cell + Fe	16.4466	–116
Mg	Cell	0.1316	–659
Mg	Cell + Mg	0.3986	+33

Table A.1 summarizes the isotopic ratios and δ values (‰) for the measured metal elements in both untreated cancer cells and cells treated with metal solutions.

A.2 Mean Isotopic ratios of metal elements across all samples

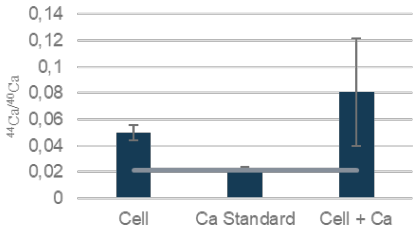

(a) Average isotopic ratio of Ca isotopes in cancer cell samples

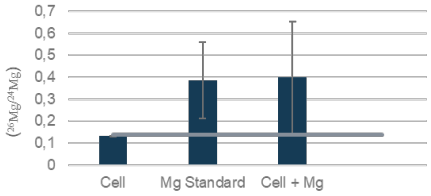

(b) Average isotopic ratio of Mg isotopes in cancer cell samples

Figure A.1: Mean isotopic ratios of $^{44}Ca/^{42}Ca$ and $^{26}Mg/^{24}Mg$ in all three cancer cell samples. The error bars represent the standard error of the mean for each value, and the horizontal lines represent the natural abundance ratios of these isotopes.

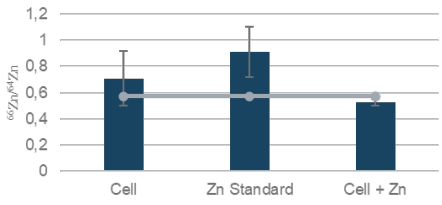

(a) Average isotopic ratio of Zn isotopes in cancer cell samples

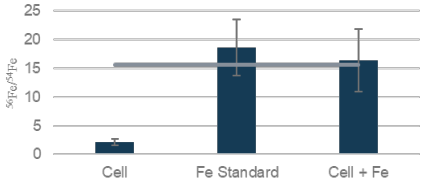

(b) Average isotopic ratio of Fe isotopes in cancer cell samples

Figure A.2: Mean isotopic ratios of $^{66}Zn/^{64}Zn$ and $^{56}Fe/^{54}Fe$ in all three cancer cell samples. The error bars represent the standard error of the mean for each value, and the horizontal lines represent the natural abundance ratios of these isotopes.

A.3 ToF-SIMS ion maps and an overlay of $C_5H_{15}NO_4P^+$ and Fe^+ signals after sputtering in chicken embryo sample A1 from group A.

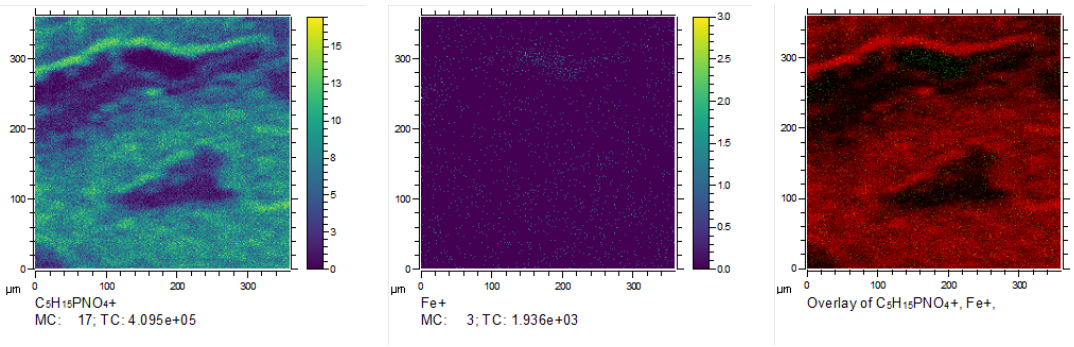

(a) $C_5H_{15}NO_4P^+$ **(b)** Fe^+ **(c)** Overlay of a and b

Figure A.3: ToF-SIMS ion maps of $C_5H_{15}NO_4P^+$, Fe^+, and an overlay of $C_5H_{15}NO_4P^+$ and Fe^+ signals after sputtering in chicken embryo sample A1 from group A.

A.4 A summary of Fe^+ and $C_5H_{15}PNO_4^+$ ion counts across Group B samples with different treatment methods

A summary of Fe^+ and $C_5H_{15}PNO_4^+$ ion counts across Group B samples with different treatment methods is shown in Table A.2. Column three shows Fe^+ ion counts and column four shows $C_5H_{15}PNO_4^+$ ion signal.

Table A.2: Summary of Fe^+ and $C_5H_{15}PNO_4{}^+$ ion counts across Group B samples with different treatment methods.

Sample	Treatment Method	Fe^+ (cts)	$C_5H_{15}PNO_4{}^+$ (cts)
B1	Fe + DMSO	1426	1,511,051
A2	Fe + DMSO, electroporated + incub	219	716,571
A3	Fe + DMSO, electroporated	89	586,926
A4	Fe, electroporated and incubated	218	1,140,412

A.5 Group C

A.5.1 Ion counts of copper isotopes and phosphocholine cation from three TOF-SIMS replicates of B1

Replicate	**$^{63}Cu^+$ (cts)**	**$^{65}Cu^+$ (cts)**	**$C_5H_{15}PNO_4{}^+$ (cts)**
Replicate 1	148,219	73,417	2,117,862
Replicate 2	42,630	17,273	1,563,727
Replicate 3	175,834	79,456	1,549,662
Average	122,228	56,715	1,743,084
Std. Dev.	70,462	34,062	325,601

Table A.3: Ion counts of ^{63}Cu, ^{65}Cu, and $C_5H_{15}PNO_4^+$ from three TOF-SIMS replicates of Sample A1, including average values and standard deviations.

A.5.2 Ion counts of copper isotopes and phosphocholine cation from three TOF-SIMS replicates of A1

Replicate	**$^{63}Cu^+$ (cts)**	**$^{65}Cu^+$ (cts)**	**$C_5H_{15}PNO_4{}^+$ (cts)**
Replicate 1	183,979	88,523	2,013,232
Replicate 2	198,634	63,619	2,296,004
Replicate 3	115,834	79,456	1,549,662
Average	126,149	77,199	1,952,966
Std. Dev.	11,554	12,604	376,803

Table A.4: Ion counts of ^{63}Cu, ^{65}Cu, and $C_5H_{15}PNO_4^+$ from three TOF-SIMS replicates of Sample A1, including updated average values and standard deviations.

A.6 Ratio of copper isotope to the phosphocholine cation for untreated samples Sample A4 and A2

Sample	**$^{63}Cu^+$ (cts)**	**$^{65}Cu^+$ (cts)**	**$C_5H_{15}PNO_4{}^+$ (cts)**
A4	14412	4020	547662
A2	10370	7824	276052

Table A.5: Ratio of copper isotope to the phosphocholine cation for untreate samples Sample A4 and A2.

DEPARTMENT OF SOME SUBJECT OR TECHNOLOGY
CHALMERS UNIVERSITY OF TECHNOLOGY
Gothenburg, Sweden
www.chalmers.se

CHALMERS
UNIVERSITY OF TECHNOLOGY